Modelling mangrove-mudflat dynamics with a coupled individual-based-hydro-morphodynamic model

Beselly, S. M.; Grueters, U.; van Der Wegen, M.; Reyns, J.; Dijkstra, J.; Roelvink, D.

DOI
10.1016/j.envsoft.2023.105814

Publication date
2023

Document Version
Final published version

Published in
Environmental Modelling and Software

Environmental Modelling and Software 169 (2023) 105814

Contents lists available at ScienceDirect

Environmental Modelling and Software

journal homepage: www.elsevier.com/locate/envsoft

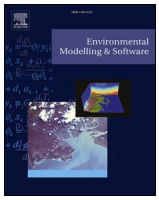

Modelling mangrove-mudflat dynamics with a coupled individual-based-hydro-morphodynamic model

S.M. Beselly [a,b,e,*], U. Grueters [c], M. van Der Wegen [a,d], J. Reyns [a,b,d], J. Dijkstra [d], D. Roelvink [a,b,d]

[a] Department of Coastal & Urban Risk and Resilience, Coastal Systems & Engineering and Port Development, IHE Delft Institute for Water Education, Westvest 7, 2611AX, Delft, the Netherlands
[b] Department of Hydraulic Engineering, Section Coastal Engineering, Delft University of Technology, Stevinweg 1, 2628 CN, Delft, the Netherlands
[c] Institute of Plant Ecology, Justus Liebig University, 35392, Giessen, Germany
[d] Deltares, 2629 HV, Delft, the Netherlands
[e] Department of Water Resources Engineering, Brawijaya University, Malang, 65145, Indonesia

ARTICLE INFO

Keywords:
Mangrove dynamics
Sediment dynamics
Mangrove-hydromorphodynamic model
Individual-based mangrove model
Delft3D-FM
Mangrove modelling
Eco-geomorphology

ABSTRACT

As climate-change-driven extremes potentially make coastal areas more vulnerable, mangroves can help sustainably protect the coasts. There is a substantial understanding of both mangrove dynamics and hydro-morphodynamic processes. However, the knowledge of complex eco-geomorphic interactions with physical-environmental stressors remains lacking. We introduce a novel coupled modelling approach consisting of an individual-based mangrove (mesoFON) and a process-based hydromorphodynamic model (Delft3D-FM). This coupled model is unique because it resolves spatiotemporal processes, including tidal, seasonal, and decadal environmental changes (water level, flow, sediment availability, and salinity) with full life-stages (propagule, seedling, sapling, mature) mangrove interaction. It allows us to mechanistically simulate forest expansion, retreat, and colonisation influenced by and with feedback on physical-environmental drivers. The model is applied in a schematized mixed fluvial-tidal deltaic mangrove forest in dominantly muddy sediment inspired by the prograding delta of Porong, Indonesia. Model results successfully reproduce observed mangrove extent development, age-height relationship, and morphodynamic delta features.

1. Introduction

Climate change-driven extremes are associated with unprecedented weather changes like a stronger wave climate, frequent storm surges, and coastal flooding (Cooley et al., 2022; Wong et al., 2014). Globally, this will increase the vulnerability of the coasts with their coastal ecosystems and more than 600 million people (Kirezci et al., 2020; Magnan et al., 2022; Merkens et al., 2016; Temmerman et al., 2023). Traditionally, coastal areas are protected by man-made infrastructure that needs continuous and costly maintenance (Cheong et al., 2013; Duarte et al., 2013; Temmerman et al., 2013). More recently, the potentially more sustainable and cost-effective Nature-based Solutions (NbS) approach has been proposed for climate change adaptation (Cooley et al., 2022; Hijuelos et al., 2019; Narayan et al., 2016). The NbS — including mangrove ecosystems — play a pivotal role in climate adaptation by enhancing coastal resilience through the utilisation of eco-geomorphological processes that naturally adapt to changing environmental forcing while being multifunctional and relatively cost-effective (Borsje et al., 2011; Chen et al., 2016; Temmerman et al., 2023). Mangroves can contribute to sustainable coastal protection in the face of climate change (Krauss et al., 2008), increasing coastal resilience regarding vertical (Norris et al., 2021) and lateral erosion (Pennings et al., 2021).

The knowledge of the contribution of mangroves to hydrodynamic processes has been relatively well appreciated and understood. Much research has been conducted to understand how the extensive rooting

* Corresponding author. Department of Coastal & Urban Risk and Resilience, Coastal Systems & Engineering and Port Development, IHE Delft Institute for Water Education, Westvest 7, 2611AX, Delft, the Netherlands.
E-mail addresses: s.besellyputra@un-ihe.org, s.m.beselly@tudelft.nl, sebrian@ub.ac.id (S.M. Beselly), uwe.grueters@bot2.bio.uni-giessen.de (U. Grueters), m.vanderwegen@un-ihe.org, mick.vanderwegen@deltares.nl (M. van Der Wegen), j.reyns@un-ihe.org, j.a.h.reyns@tudelft.nl, johan.reyns@deltares.nl (J. Reyns), jasper.dijkstra@deltares.nl (J. Dijkstra), d.roelvink@un-ihe.org, j.a.roelvink@tudelft.nl, dano.roelvink@deltares.nl (D. Roelvink).

https://doi.org/10.1016/j.envsoft.2023.105814
Received 3 April 2023; Received in revised form 17 June 2023; Accepted 25 August 2023
Available online 28 August 2023

systems, trunks, and lower part of the canopy slow down the water flow, attenuate waves, and thereby in the calm period, facilitate the deposition of fine sediments (Alongi, 2008; Mazda et al., 1997; Norris et al., 2021). Some studies show the potential of mangroves as a buffer to large, infrequent disturbances such as tsunamis (Dahdouh-Guebas et al., 2005; Kathiresan and Rajendran, 2005), storms (Das and Vincent, 2009; Fairchild et al., 2021), and coastal flooding (in combination with levees) (van Wesenbeeck et al., 2017). Environmental conditions, in their turn, influence the mangrove dynamics. Elevated intertidal mudflats allow mangroves to develop, whereas sediment deficits may erode coasts and mangrove belts. Varying temperatures, salinity levels, and bed elevation can change the mangrove community composition or structure over time (Alongi, 2008; Duke et al., 1998; Lugo and Snedaker, 1974; Osland et al., 2017; Woodroffe, 1992).

In reality, mangrove systems will develop in complex, species-specific feedback processes with forcing conditions and environmental evolution. For example, mangroves will attenuate waves, which facilitates deposition and bed elevation impacting again on mangrove growth/starvation. However, uncertainty remains given the high-non-linearity (Barbier et al., 2008; Murray et al., 2019) and critical failure threshold (Spalding et al., 2014; van Hespen et al., 2022b) of the mangroves. These spatiotemporal variations make quantifying the functional capacity of mangroves a challenge (Temmerman et al., 2023).

Ideally, resolving the contribution and interactions of mangroves with the physical stressors requires a detailed, spatially explicit modelling approach that covers all mangrove characteristics and life-stages (Dahdouh-Guebas et al., 2022; van Hespen et al., 2022a), where it is currently lacking. The most widely used modelling tools in resolving mangrove-ecogemorphological interactions are spatial and statistical models, followed by process-based and conceptual models (Rivera-Monroy et al., 2022). Pretzsch (2009), van Maanen et al. (2015), and Xie et al. (2020) provide examples of dynamic models that cover the forest-scale characterized by a top-down hierarchy where the growth is prescribed based on specific physical-environmental stress for each 'numerical cell' at a specified time. Only a few numerical models include physical-ecological processes, e.g., interactions between mangroves and waves, tides, and sediment dynamics in mangrove forests (Buffington et al., 2021; Fanous et al., 2023; Rodríguez et al., 2017; van Maanen et al., 2015; Willemsen et al., 2016). These grid-based approaches apply grid-averaged dynamics that may not reflect the actual mangrove dynamics (Berger and Hildenbrandt, 2000).

In contrast, Individual-Based Models (IBM) use a tree-centred or bottom-up approach leading to the detailed capture of species ranges, forest structure, biomass, and system behaviour (Wang et al., 2014). Examples are MANGRO (Doyle et al., 1995), FORMAN (Chen and Twilley, 1998), and KiWi (Berger and Hildenbrandt, 2000). Further development of mangrove IBM models is MesoFON (Grueters et al., 2014), adding crown plasticity to include in tree competition, BETTINA (Peters et al., 2014), which includes mangrove feedback to salinity, and MANGA (Bathmann et al., 2020) with plant groundwater-salinity feedback. Forest expansion depends on the successful seedling establishment (Shih et al., 2022; van Hespen et al., 2022a). However, treatment of rejuvenation in IBMs is still insufficient to simulate the establishment of a mangrove ecosystem as it depends on the dispersal of propagules. Propagule dispersion is critical for colonising and regenerating mangrove forests (Zainol et al., 2022). The dispersal mechanism is mainly attributed to hydrodynamic processes (Duke et al., 1998; Shih et al., 2022), which is not covered by the models mentioned. Although the IBM models have the capability to simulate the feedback to specific physical-environmental drivers, most of them assume a constant physical-environmental driver in time with spatial limitation to a local scale or a few hectares.

This study aims to develop a model that explicitly solves the hydrodynamic and morphological processes and their spatially explicit interactions with an individual-based mangrove dynamics model. Developing such a mangrove-ecosystem model requires a multi-modelling approach (Dahdouh-Guebas et al., 2022; Rivera-Monroy et al., 2022). This integration of multiple models includes the coupling of hydrodynamic (flow-waves), sediment transport, nutrient transport, and vegetation dynamics models. The proposed modelling approach benefits from the detailed forest structure provided by IBM (MesoFON) to parameterize the physics of mangroves to the hydro-morphodynamic model (Delft3D-FM), while IBM can use spatiotemporal physical-environmental changes simulated from the hydro-morphodynamic model. This approach can readily be expanded to the forest and ecosystem development at the landscape/regional scale. It will provide a full life-stage interaction (propagule, seedling, sapling, mature tree) depending on variations in inundation depth, bed level, and salinity.

In a schematized way, the proposed modelling approach is validated against a real-life case study of the prograding delta in Porong, East Java, Indonesia, resulting from an upstream mud volcano outburst (Beselly et al., 2021). Porong Delta has been experiencing unprecedented sediment load due to the mud volcanic eruption with a factor of 3–4 compared to before the eruption (Jennerjahn et al., 2013). This extreme condition has promoted rapidly prograding delta along with mangrove belt development (Sidik et al., 2016). First, we assess our model performance by its ability to reproduce the development of the long-term pattern in the observed mangrove extent and age-height relationship. Second, evaluate the pattern of mangrove growth, seedling dispersal/reproduction, and mangrove extent in response to varying sediment concentration, river discharge, and salinity distribution.

2. Methods

2.1. Model description

In a so-called hybrid modelling approach (Vincenot et al., 2016), we couple the landscape-scale process-based hydromorphodynamic Delft3D-Flexible Mesh (DFM) model (Deltares, 2021) and the individual-based MesoFON (MFON) mangrove model (Grueters et al., 2014). By coupling these two model paradigms, the coupled model DFMFON generally encompasses: 1) the establishment of an individual-based mangrove community by propagule import from simulated hydrodynamics, 2) the expansion of mangrove belt in mutual interaction with a hydro-morphodynamic model including bed level development, and 3) the persistence of mangrove forest by regeneration and rejuvenation of individual mangrove trees after environmental changes such as varying salinity levels and other hydrodynamic growth conditions.

2.1.1. Coupling procedure

As indicated in Fig. 1, DFM calculates hydrodynamic processes (waves, tides, and river discharge), sediment transport, and resulting morphodynamic development with a maximum hydrodynamic time step of 200 s. At each time-step, DFM calculates the bulk drag coefficient induced by mangrove trees. At the coupling interval of 90 days, the coupling interface translates DFM grid-based variables (water levels, salinities, and bed levels) into MFON tile-based salinity and Window of Opportunity (WoO) (Balke et al., 2011) maps. Additionally, the coupling interface generates propagule dispersal pathways from two-week DFM averaged tidal flow patterns. Based on these data, MFON updates the mangrove stands in a 90-day mangrove dynamics run. The coupling interface then translates the new MFON-generated mangrove stands into a DFM grid-based drag coefficient field for the following 90-day DFM run. In the outer coupling, belowground biomass bed level change is calculated. The 90-day coupling interval was chosen to allow for seasonal fluctuations of the local climate (wet and dry seasons) and to realistically incorporate the reproduction of mangroves, such as flowering, fruiting, and seedling production. As the real case study location is fully inundated within the tidal range, we assumed the (porewater) salinity effect on mangrove growth equals surface seawater salinity. We

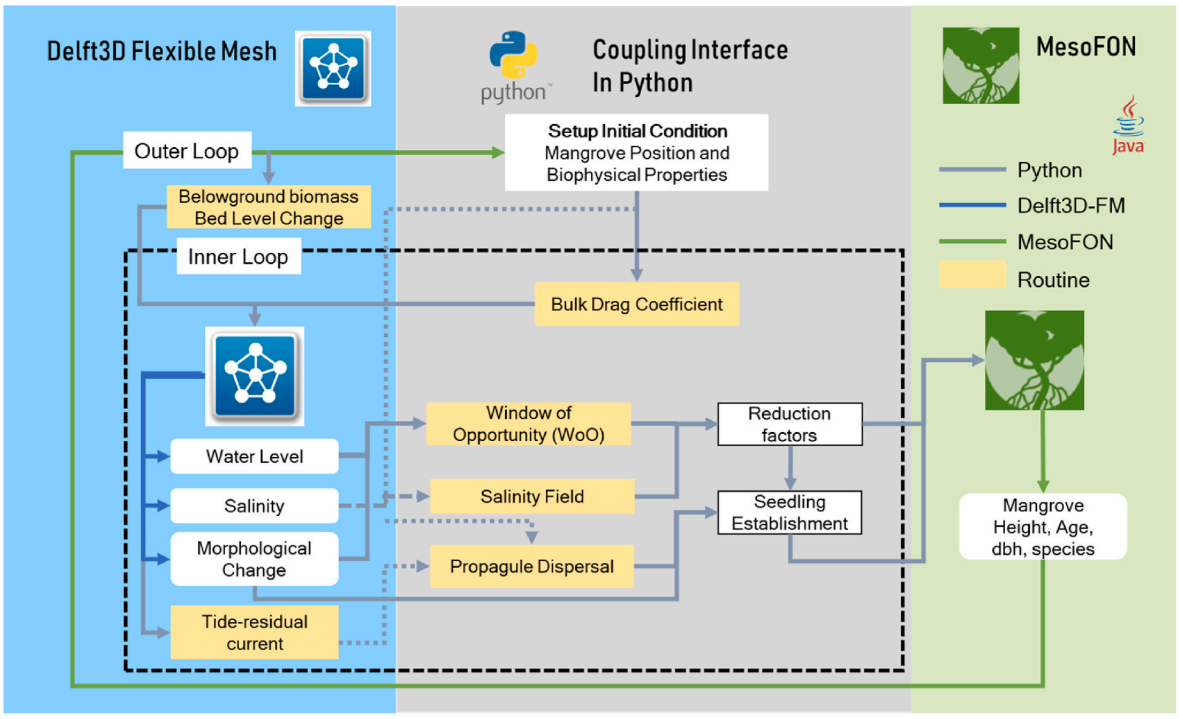

Fig. 1. Overview of the coupled DFM-MFON model.

presume an optimum condition for the mangrove growth, not depending on nutrient availability or other water quality aspects like pH level and hydrogen sulphide concentration.

The coupling interface is developed in Python 3.9.7 and applies the Basic Model Interface (BMI) module (Hutton et al., 2020). BMI enables the efficient retrieval and update of DFM variables (i.e., water levels, velocities, salinities, drag coefficients, and bed levels). Through this, the model represents the full mangrove life stage and interactions with ecological and physical drivers at each stage.

2.1.2. Entities and state variables

The model comprises single-species mangrove stands, and tiled landscape area maps as entities. The state variables of the trees in MFON were defined by the life stage (propagule, seedling, sapling, and mature tree), the species and biophysical properties: position, dbh (m), and height (m). The physical or hydro-morphodynamic drivers in DFM were defined as water level (m), salinity (ppt), spatial plant drag coefficient, water velocity (m/s), and bed level (m). The MFON tree environment was represented by 200 × 200 m tiles from the DFM domain to prevent overloading each IBM with excessive numbers of individuals and to obtain the most optimum computational efficiency for individual-based simulation. The spatially varying salinity and WoO probability calculated in Python were converted to rasters and tiles (Fig. 2).

2.1.3. Models

2.1.3.1. Delft3D-Flexible Mesh (DFM) Hydro-morphodynamic model. We applied a state-of-the-art, process-based, open-source DFM in 2DH to solve the relevant hydro-morphodynamic processes and their spatio-temporal variations in the coastal, riverine, and estuarine areas (Deltares, 2021). DFM employs unstructured grids (triangles and quadrangles) to resolve shallow water equations under the Boussinesq assumption with a finite volume method. With the D-Flow module as its core for the hydrodynamic conditions (e.g., velocities, water elevations, and salinity), the DFM model is designed to interact with other DFM modules, e.g., D-Waves for wave modelling, D-Morphology for sediment transport and morphology. Additionally, DFM applies the BMI that enables initialising, running, retrieving, and altering parameters' values in standard interface calls (Fig. 3).

Mangrove systems are characterised by high turbulence, sometimes equivalent to the observed value in the surf zones (Norris et al., 2017), and well-mixed conditions that can be represented in the two-dimensional depth-averaged (2DH) model (Horstman et al., 2015). DFM separates the vegetation-induced resistance λ and bare bed

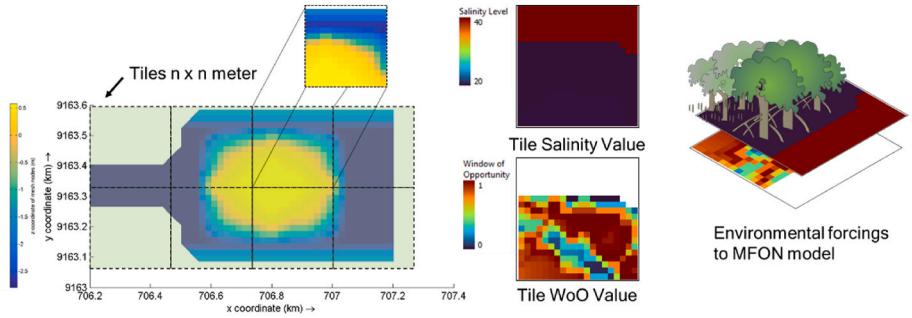

Fig. 2. A schematic for retrieving and processing the variables of the DFM model. The (processed) values are converted into raster. The rasterised parameters were tiled and used as input for the MFON model.

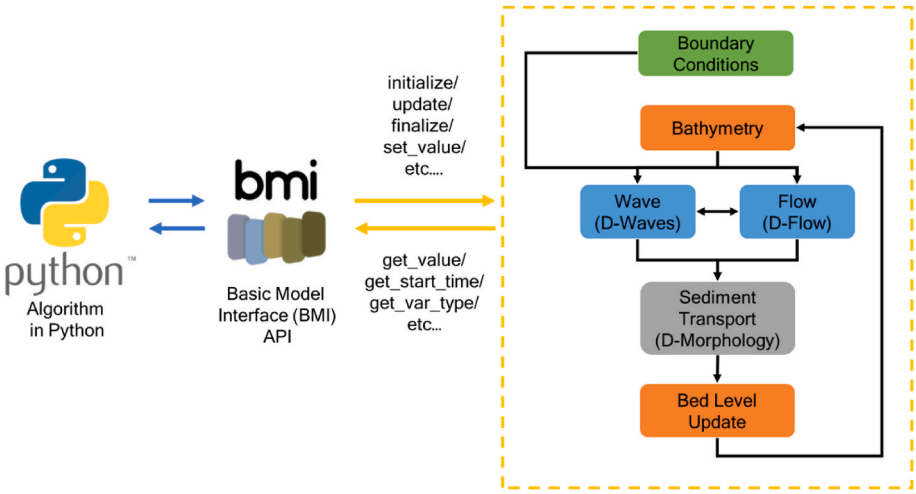

Fig. 3. Overview of DFM full morphological loop model structure with the commonly used online coupled modules and BMI API function call in Python. The complete BMI functions for DFM can be explored at https://svn.oss.deltares.nl/. The BMI wrapper for the DFM model can be downloaded from the OpenEarth repository at https://github.com/openearth/bmi-python.

roughness C ($m^{1/2}/s$) in the momentum equation (Deltares, 2021). The modified Baptist (Baptist et al., 2007) representative C and λ formula (Eq. (1) and Eq. (2)) requires information on the height of vegetation h_v (m), density n (number of trees/m^2), bulk drag coefficient (C_D), and bare bed roughness (C_b) for each grid cell. The calculated C_D will be used to estimate the mangrove-induced drag in the DFM model, whose implementation is provided in section 2.1.4.1.

$$C = C_b + \frac{\sqrt{g}}{\kappa}\ln\left(\frac{h}{h_v}\right)\sqrt{1+\frac{C_D n D h_v C_b^2}{2g}} \quad (1)$$

$$\lambda = \frac{1}{2}C_D n D \frac{h_v}{h}\frac{C_b^2}{C^2} \quad (2)$$

where h is water depth (m), κ is the dimensionless von Kármán constant, and D is stem diameter (m).

2.1.3.2. MesoFON (MFON) mangrove model. The overall purpose of the MFON model (Grueters et al., 2014) has been to simulate individual mangrove growth based on tree-to-tree competition and environmental conditions. The MFON model simulates up to ten mangrove species. The tree competition is based on the Field of Neighbourhood (FON) approach (Berger and Hildenbrandt, 2000). FON represents the radius of competition of each tree either above or below ground, where the strength of influence one tree exerts on another depends on the distance to the other tree (Fig. 4) and the diameter of influence is related to the stem diameter. The recruitment and establishment in this study were updated and evaluated in the coupling interface to reflect the specific hydrodynamic conditions. MFON has the mangrove tree entity where crown plasticity is the most important process (deactivated in this study). MFON tree mortality processes depend on local disturbance events and in case of no growth in dbh averaged over five years. The most important design concept of MFON is how the mangrove tree senses and recognises the influence of neighbouring trees via its above- and below-ground FON.

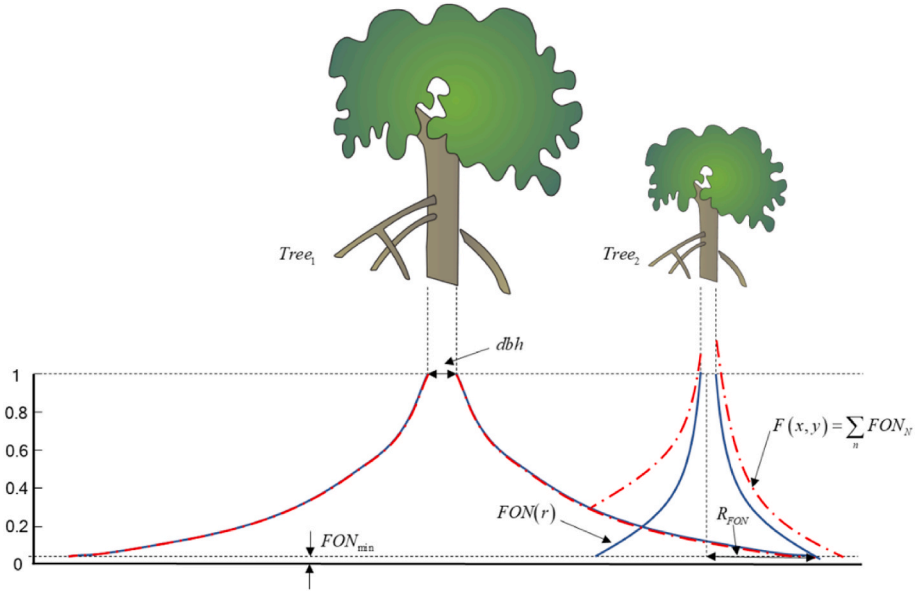

Fig. 4. FON illustration as in MFON. It shows the intersecting FONs of two neighbouring trees ($Tree_1$ and $Tree_2$); the influence of Tree2 on Tree1 depends on the tree's size and how far the distance of each tree is.

2.1.4. Coupling interface

Mangroves interact with the environment and provide feedback dependent on the three factors that predominate physical processes, i.e., nutrients, salinity, and sea level/hydroperiod (Grueters et al., 2014; Krauss et al., 2014; Wimmler et al., 2021). These factors are intertwined and affect the growth of mangrove trees, regulate species distribution and the zonation within the mangrove forest, and ultimately determine the productivity and extent of the mangrove ecosystem. The porewater salinity distribution (Lovelock et al., 2006; Piou et al., 2006) impact mangrove growth, and the spatial expansion depends on the tidal flooding and duration (Balke et al., 2015; Lovelock et al., 2015). These factors determine the mangroves' growth, dieback, and seaward expansion (through tree recruitment).

2.1.4.1. Drag parameterisation. An accurate drag parameterisation is essential since the C_D value in mangrove forests depends on tree species and the root composition/geometries (Mullarney et al., 2017), which varies over the water depth. However, considering the 2DH simulation, a bulk drag predictor was preferred. Therefore, we parameterised the presence of the mangroves as the bulk drag coefficient (C_D) using the formulations by van Maanen et al. (2015). This approach assumes that the drag force exerted on the mangroves depends on the vegetation length scale (L) in Eq. (4) as a function of the obstacles' projected area (A) and the obstacles volume (V_M) in a control volume (V). Eq. (3) was defined as the total of $C_{D,no}$ (drag coefficient of the bare surface) that was set to a value of 0.005. A dimensional constant e with a value of 5 m is set to attain a realistic drag coefficient, as proposed by van Maanen et al. (2015).

$$C_D = C_{D,no} + \frac{e}{L} \tag{3}$$

$$L = \frac{V - V_M}{A} \tag{4}$$

The definition of obstacles volume (V_M) varies between species and hydroperiod. Therefore, we simplified the trunk as a truncated cone, with a diameter at the base d_0 and a diameter at each water depth d_{wd} derived from the species-specific diameter-height allometric relationship (Berger and Hildenbrandt, 2000) following the mangrove's age. Furthermore, mangroves have different rooting systems, i.e., pneumatophores of *Avicennia* spp., root knees of *Bruguiera* spp., and plank roots of *Kandelia* spp. Therefore, we simplified the rooting systems (Fig. 5) as cones (Eq. (5)), cylinders (Eq. (6)), and prisms (Eq. (7)), respectively (Du et al., 2021; Mazda et al., 1997, 2006).

$$V_{M,avicennia} = \sum_{i=1}^{n} \frac{\pi D_i^2 H_i}{12} \tag{5}$$

$$V_{M,brugueira} = \sum_{i=1}^{n} A_i H_i \tag{6}$$

$$V_{M,kandelia} = \sum_{i=1}^{n} A_i H_i \tag{7}$$

2.1.4.2. The window of opportunity for propagule establishment. The effect of hydroperiod was taken into account by the concept of Window of Opportunity (WoO) (Balke et al., 2011). WoO describes the minimum disturbance-free period as a critical duration that allows seedling establishment. This disturbance-free period is defined by the time series of external forcing, e.g., tidal water level and waves. Balke et al. (2015) indicate that five inundation-free days are required for *Avicennia marina* to let the propagule's root securely anchor with a length of 1.6 cm. Before that, two days of root growth resulting in 0.5 cm length are essential to prevent seedling toppling due to inundation with no waves. We calculate the WoO probability by taking the daily maximum water level in each cell of Delft3D-FM to find the minimum three days inundation free period and calculate the probability.

2.1.4.3. Propagule production and tree recruitment. The reproduction phase of *Avicennia marina* trees is characterised by peak propagule production during the wet season (Almahasheer et al., 2016; Jiménez, 1992) with an obligate dispersal of one to two weeks (Booker et al., 1998; Clarke, 1993; Rabinowitz, 1978). Reports mentioned propagules could float up to several months and remain viable, for example, *R. apiculata* and *R. mucronata* in Micronesia, three months and five months, respectively (Drexler, 2001), and *B. sexangula* in Hawai'i (2 months) (Allen and Krauss, 2006). *Avicennia* spp trees in the study area (Porong Estuary) are estimated to start producing propagules at the age of 3–4 years (Anwar and Gunawan, 2006; Sidik et al., 2013; Wirjoadmodjo and Hamzah, 1982). In the model, we parameterised the propagule production to occur in January (Anwar, 2006; Tala, 2020) for mangrove trees older than four years. The number of propagules produced by a tree per year (N) follows this equation:

$$N = f_{red,P} \times f_{red,sal} \times D \times A \tag{8}$$

where $f_{red,P}$ and $f_{red,sal}$ are the reduction factors due to nutrient availability and salinity, respectively. D is the species-specific seedling density per crown surface area A, which is assumed to have a value of 0.06 ($1/m^2$). The $f_{red,P}$ is held constant with the value of 1 during the simulation (Grueters et al., 2019), assuming the nutrient availability is suitable for optimum growth, while the varying $f_{red,sal}$ is dependent on the seawater salinity map obtained from hydrodynamic simulation and is calculated as:

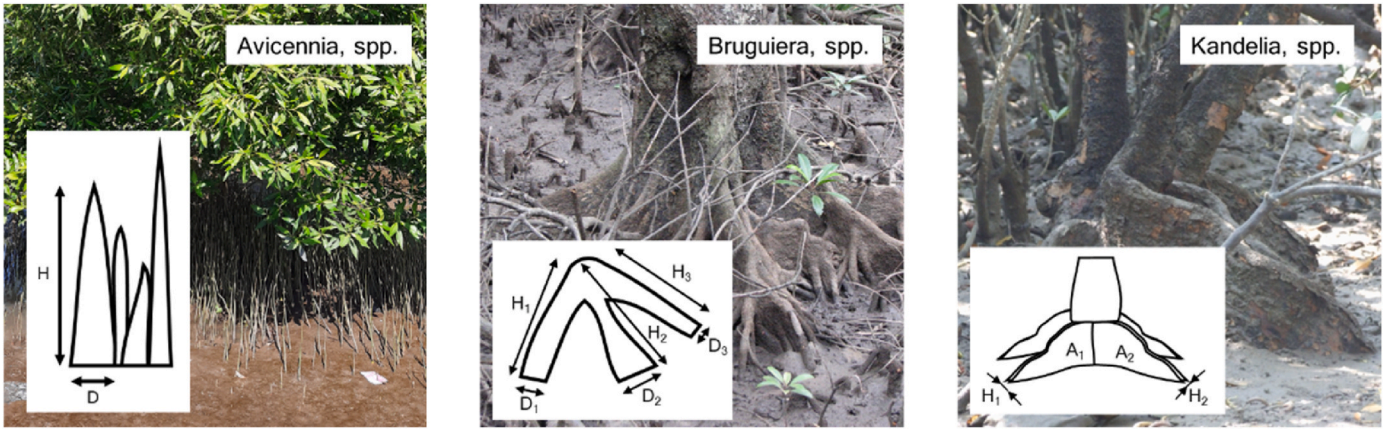

Fig. 5. Simplification of the rooting systems and the parameterisation for bulk drag coefficient calculations.

$$f_{red,sal} = \frac{1}{1 + \exp(d(U_i - U))} \quad 9$$

Where U is the salinity value in ppt, d is a constant that determines the decline of $f_{red,sal}$ with increasing salinity (−0.18 for *Avicennia* spp.). The constant U_i is the salinity at which $f_{red,sal}$ is 0.5 (72.0 ppt for *Avicennia* spp.) (Chen and Twilley, 1998). The salinity factor is considered important as high salinity values likely reduce propagule reproduction or dispersal (Lovelock et al., 2017). In the model, the salinity value is determined by taking the median value from the DFM model on each cell during the coupling period.

At first, the propagules are uniformly distributed (Srivastava and Khamis, 1978) along the area of the crown surface at $Pos(x,y)_n$. Next, as *A. marina* propagule is buoyant (Van der Stocken et al., 2019) and able to float irrespective of salinity (Clarke et al., 2001), local propagule dispersal around the parental tree depends on the magnitude and direction of the current without the influence from the wind. The propagule dispersal is only calculated for the first two weeks after release, considering the minimum inundation-free period for *Avicennia* spp. to achieve the early anchorage of the propagules (Balke et al., 2015) obligate for seedling establishment. We calculated the average tidal current ($\overrightarrow{u}$) over the two weeks of simulation days to determine the transport pathway of propagules. Assuming the tidal current is the dominant process over the propagules buoyancy properties (Di Nitto et al., 2013), the final position ($Pos(x,y)_{final}$) can be formulated as:

$$Pos(x,y)_{final} = Pos(x,y)_n + \overrightarrow{u} \times dt \quad 10$$

The survival of the spatially distributed propagules is then evaluated by considering the tidal inundation period P_{WoO} and sediment disturbance $S_{disturb,sed}$ (burial due to sediment and uprooting due to erosion) following the WoO (Balke et al., 2015). Finally, the surviving seedlings are allowed to grow in their final position until sapling age (two years) and are subsequently transferred as saplings to the MesoFON module. We close the life cycle of the mangroves by introducing the propagules and seedlings. This is a novel contribution to the mangrove stand models since previous ones such as FORMAN (Chen and Twilley, 1998), KiWi (Berger and Hildenbrandt, 2000), and MesoFON (Grueters et al., 2014) simulated tree recruitment as saplings, except for MANGRO (Doyle et al., 1995) that simulated it as seedlings. Additionally, forest expansion is driven by the successful seedling establishment.

2.2. Experimental design

2.2.1. Case study

The schematized model was set based on the physical characteristics of the prograding Porong Delta in Indonesia (Fig. 6c). Porong Delta has been experiencing rapid progradation due to high sediment load from the diverted mud volcano outburst. We initiated the domain based on the northern delta lobe's geomorphological characteristics in 2016, as described by Beselly et al. (2021). In this period, the delta lobe was just emerged and was naturally colonized by the mangroves, even though mangrove planting activity was conducted in 2017. We collected a decade of daily river discharge, water level observation, and a series of campaigns of sediment sampling, bathymetry, sediment concentration, tidal, and waves. Mangrove observations were conducted in 2010, 2011 (Setiawan et al., 2019) and updated in 2019 (Beselly et al., 2021) and 2021.

2.2.2. Model parameterisation and schematisation

Fig. 6d shows the schematized model consisting of a 1500 m long funnel-shaped estuary with a river mouth converged from 140 m at the landward head to 500 m at the end of the basin. The river channel area was defined as a rectangular polygon with a length and width of 240 m and 140 m, respectively, followed by a delta area with the dimension of 500 m × 640 m, where the 120 m triangular-shaped polygons are in the transition. This domain's configuration comprised grid cells with a size of 20 m. The initial bathymetry was prescribed with the presence of the delta lobe in the middle of the estuary to quickly start the delta development and attain the dual channel (north-south) system as observed in the field. It has a depth of −2.8 m in all domains, with 0.8 m at the crest of the lobe. The erodible banks, river, and seabed have an initial sediment thickness of 30 m. The sediment consists of mud. We used a uniform value of Chézy roughness 65 $m^{1/2}/s$ to represent the soft bed of cohesive sediment in the condition without vegetation.

We forced the model with two open boundaries: (seasonal) fresh water river discharge at the landward end and tidal water level variation at the seaward boundary. Because of the low prevailing significant wave height, we did not include wind-generated waves in the schematized model. The river boundary was set as the only boundary to supply sediment and schematized to flow the discharge of 0 or 35 m^3/s during the dry season (June to November) and 150 m^3/s during the wet season (December to May) following the average seasonal discharge as observed. The seaward boundary has a semi-diurnal M2 signal with an amplitude of 1.2 m and an initial salinity of 25 ppt, as the tidal range in

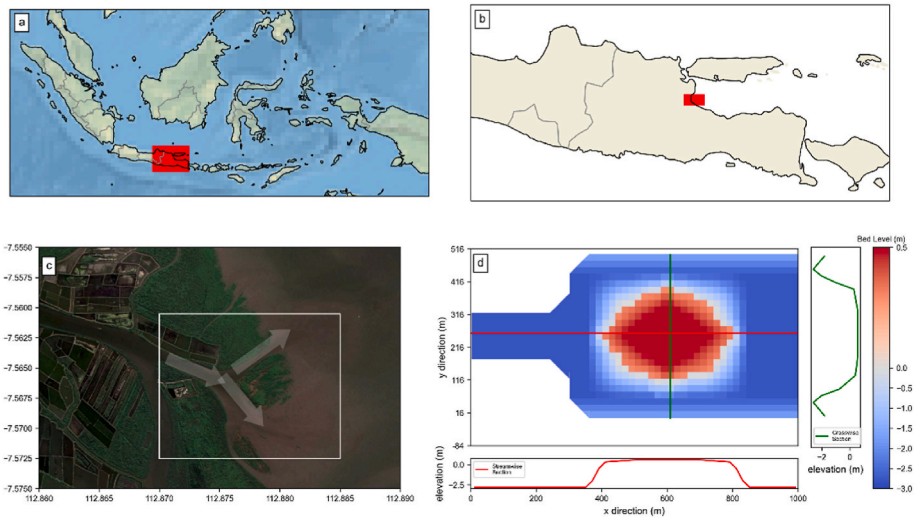

Fig. 6. The real case study is located in Indonesia (a), East Java Province (b), focusing on the northern delta lobe in Porong Delta (c), where it is schematized into a funnel shape estuarine with a delta in the middle (d). In (d), the details of the model domain, grid arrangement, bathymetric, and cross sections are presented.

the study area. A suspended sediment concentration (SSC), varying between scenarios, was defined at the river boundary with a Thatcher-Harleman time lag of 90 min. Thatcher-Harleman time lag gradually releases the concentration during the prescribed period at the river boundary to prevent sudden variation of the suspended sediment concentration on tidal flow reversal (Deltares, 2021).

A morphological factor (MF) of 30 was used in this study. It means a single hydrodynamic tide results in morphological changes of 1 month, thus reducing the computational time. In the presence of waves, a maximum MF value of 50 may be applied, whereas values up to 400 may be used without waves (van der Wegen and Roelvink, 2008). With MF = 30, three DFM simulation days equal three months or 90 days of morphological update. Thus, it will match the offline three-monthly coupling with MFON. Ultimately, two years of hydrodynamic simulation with MF can produce 60 years of morphodynamic evolution. This time scale was chosen to deal with the high computational demand of the MFON model while still having the representation of mangrove dynamics (at decadal time scale) and the (estuarine) landscape development. A detailed model setting is described in Appendix 1.

2.2.3. Initialisation

Initially, a forest plot area in the upstream part of the delta is distributed with randomly placed saplings. Next, the initial mangrove position (x and y) and uniform biophysical properties (species, diameter at breast height (dbh), and height) were prepared as a shapefile. An additional initialisation procedure was the definition of the seaward limit of the mangrove edge. Mangroves' seaward boundary is limited to the lowest low water level (LLWL) and 0.5 m additional elevation as the buffer. Next, we converted the bathymetry as a raster, clipped the raster following the seaward limit, and tiled the raster and mangrove shapefile as the MFON world. MFON parameter files were prepared for separate tiles, and the simulation can be started.

2.2.4. Scenarios

We defined eight different sensitivity scenarios as shown in Table 1. These scenarios reflect high-to-low salinity by varying river discharge quantity for each season and rich-to-poor sediment scenarios by varying the sediment concentration value. The settings are based on the actual conditions in Porong Estuary. Porong River, one of the major branches of the regulated Brantas Watershed, is equipped with a series of barrages and floodgates. These flood control structures make the river act more as a diversion channel, with almost no discharge during the dry season and high flow during the wet season. The suspended sediment concentration (SSC) in Porong River depends on the hinterland's mud disposal operation.

2.2.5. Model results analysis

We assessed the simulation results with qualitative and quantitative analyses. Qualitatively, we look at the expansion pattern of the mangrove extent during the simulation period. We examine the shape of the mangrove extent and the stand structure. The simulated patterns are compared visually with the satellite observations presented by Beselly et al. (2021). Quantitatively, we divide the analysis to explain the mangrove and estuary feedback with the hydromorphodynamic phenomena as proxies. Vegetation responds to environmental forcing in the form of biophysical property changes. For instance, the most noticeable quantity (even from medium-resolution satellite products) is the mangrove area development. First, we sorted the geo-referenced simulated trees from the tallest to the smallest. Then, the canopy area is calculated as circular from the centre of each tree's stem. When the mangroves' canopies overlap, we intersect the area and calculate the union. With this approach, the smaller trees' area is not calculated, but the top of the canopy is. This approach is similar to the satellite-based mangrove extent observation. Another noticeable quantity is the mangrove height. We use the top of the canopy height to validate the simulation with the observation. The Porong mangrove forest shows seasonal variation dynamics. Here, we use the seasonal-trend decomposition (STL) using LOESS (locally estimated scatterplot smoothing) (Cleveland et al., 1990) to decompose the spatio-temporal variability of the mangroves into the trend and seasonal components. We performed STL analysis with the statsmodel v0.13.2 package in Python (Seabold and Perktold, 2010). The STL method has been commonly used to analyse the (seasonal) time series development, e.g., nutrient concentration trend in a coastal catchment (Wan et al., 2017), mangrove biomass (Furusawa et al., 2013), and mangrove forest cover phenology (Chamberlain et al., 2021). Regarding morphodynamic analyses, we compared the bed level with and without mangroves for each scenario. We also analysed the morphodynamic development and hydrodynamic responses in the vegetated domain.

Table 1
Sensitivity scenarios on seasonal variation in mangrove development.

Scenario	Discharge (m^3/s)		Concentration (kg/m^3)		Condition
	Wet	Dry	Wet	Dry	
A	150	0	0.05	0	Hi Sal, Rich Sed (base scenario)
B1	150	0	0.03	0	Hi Sal, Med Sed
B2	150	0	0.01	0	Hi Sal, Poor Sed
C	150	35	0.05	0	Low Sal, Rich Sed
D1	150	35	0.03	0	Low Sal, Med Sed
D2	150	35	0.01	0	Low Sal, Poor Sed
E	150	35	0.05	0.01	Low Sal, Rich Sed (Wet and Dry)
F	150	35	0.03	0.01	Low Sal, Med Sed (Wet and Dry)

3. Results

3.1. Mangrove-morphodynamic responses and feedback loop: general pattern

At the beginning of the simulation, we started all scenarios with a small patch of homogeneous *Avicennia marina* stands in the upstream part of the delta. To simulate the natural colonisation, we adopted a sparse saplings' density of $0.03/m^2$, as observed in the case study location. These saplings have homogenous biophysical characteristics with 1.37 m height and 0.096 m dbh at the age of 1 year. The initial mangrove area covers around 8% of the delta area above the lowest low water level. The simulation results indicate approximately three major phases in the general development of the mangrove dynamics. These phases are discriminated from visual analysis of the DFM-MFON model results (Fig. 7 and Appendix 2) and the mangrove area (Fig. 8). Phase 1 represents the first 15 years of development (year 0 to year 15), Phase 2 represents years 15–30, and the final Phase 3 represents years 30–60. The developments' division is clearly seen from slope changes and the spread of the scenario pathways, as in Fig. 8. Please refer to Appendix 2 for all scenario plots and Supplement 1 for the animations.

In the first phase of the simulation, mangroves tend to colonise the available space in the delta lobe, which is related to the available accommodation space. Mangroves expand and fill the space until they reach the physical limit (mean sea level). The gradual distribution of mangrove stands reflects older trees in the interior and younger trees at the fringe.

After about 15 years, the rate of mangrove area expansion has increased for every scenario compared to the initial years (Fig. 8). The reason is that the mangrove population has matured and started producing more propagules. The available accommodation space in the platform begins to be filled with the propagules transported by the current. After that, in phase three, the propagules start to disperse outside the delta or into the allowable area along the northern and southern channels triggering mangrove establishment outside the delta (Fig. 7).

Since the production of propagules correlates with the biophysical properties, the mangrove stands' height and age distribution affect the

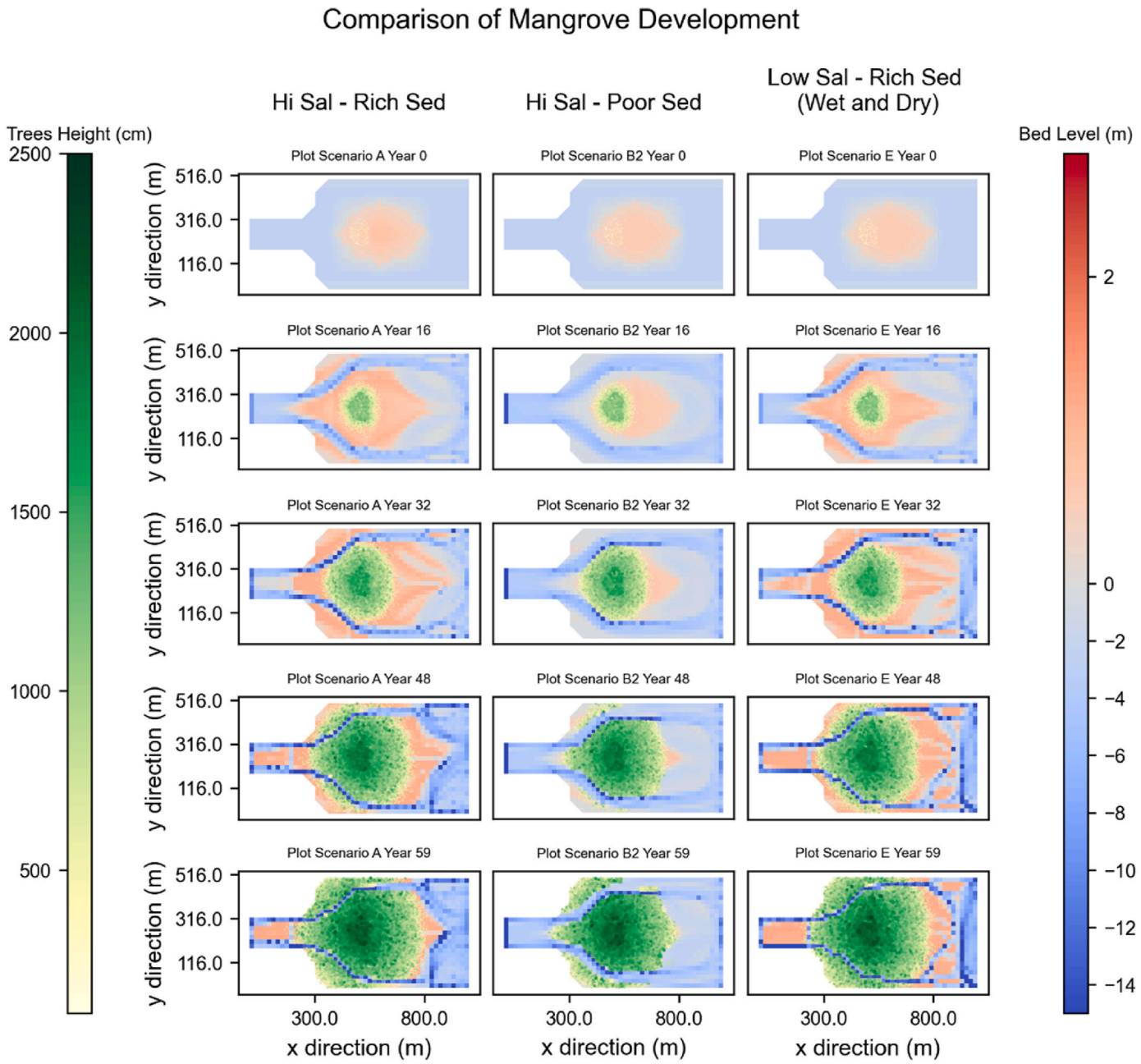

Fig. 7. Snapshot of mangrove development from selected scenarios representing extreme environmental conditions (high-low salinity) and sediment availability (rich-poor sediment availability). In the scatter plot, the size of a tree is relative to its diameter; a larger circle implies a wider tree diameter. With this, we can examine the distribution and structure of the mangrove stand where the darker green scatter has older and taller trees.

mangrove expansion pattern. Initially, more propagules are produced by the mature trees in the interior rather than by the younger population at the fringes. A mature tree is defined (Wilson, 2020) by the change from the non-flowering (juvenile) stage to the flowering (mature) stage. The number of propagules dispersed is more concentrated in the interior. Thus, the propagules drifting outside the delta remain few. As competition in the interior increases (Fig. 9), successful recruitment in the interior becomes limited, but the mature mangroves at the fringes easily disperse the propagules around the delta. After 30 years, the newly established mangrove population adjacent to the northern and southern channels initiates the life cycle and even occupies the accommodation space inland.

Phase 2 and phase 3 show the contribution of sediment availability. In contrast to the slightly different pathway described in the mangrove's area development in phase 2, the top of the canopy parameter indicates a significant role in sediment availability. In contrast to poor sediment scenarios, rich sediment scenarios provide more accommodation space, less competition for space, and, therefore, an increase in the distribution of the higher mangrove stands. The higher sediment concentration scenarios create a wider and more elevated intertidal area. At the beginning of phase 3, a transition is observed with rich sediment scenarios having a higher mangrove population. It is noted that with the highly saturated mangrove population in the delta, the competition for space increases (Fig. 9).

As the mangroves grow and reproduce, larger mangroves have wider FON related to stem diameter and tree height (Fig. 4). Due to reproduction in the denser mangrove stands, the intersecting FONs raise the strength of influence one tree exerts on another. Hence, the intra-specific competition (competition within the same species in the same plot) value shown in Fig. 9 increases over time. The mangrove population in

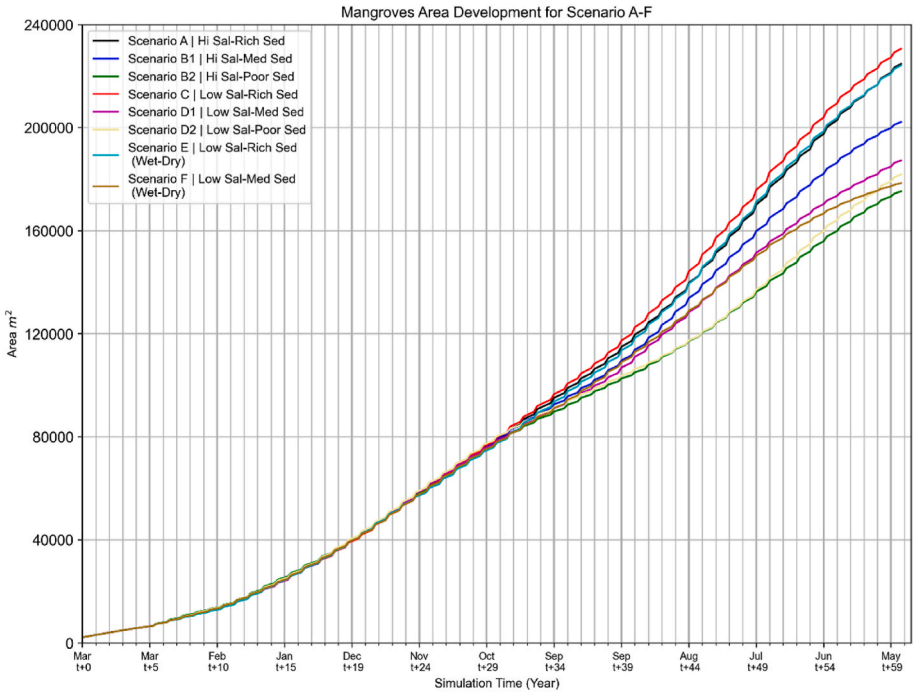

Fig. 8. Simulated mangrove area development for 60 years of simulation.

the middle of the delta showed the most noticeable increasing pattern as the model was initialized in these tiles. The effect of high competition, a smaller WoO, and limited propagule dispersal have triggered dieback of the younger stands, as illustrated by the bend of northern channel and the centre of the southern channel. One can see the peak of the competition between year 40 and year 50 and the decline in the following years. In these tiles, the propagules were initially dispersed close to the fringing parental trees due to limited accommodation space. As a result of the higher competition, young trees are more likely to die off. In the next phase, mature trees located inland and those surviving grow with a lower competition resulting from the preceding dieback and the sedimentation facilitated by the reduced flow velocities in the forest. As reproduction restarts, the competition begins to increase.

The seasonal influence on the competition shows up as a cyclic pattern over the year. We observed the lowest competition at the beginning of the wet season and the peak of competition at the middle and the end of the dry season. The low competition value in the wet season is likely related to the dieback of some mangroves due to the strong competition in the dry season of the previous year and relatively favourable conditions during the wet season. With the optimal growth of the mangroves during the wet season and simultaneous increase in density due to propagule production, the trees experience the highest competition value during the dry season.

The schematized model can qualitatively reproduce the observed expansion pattern in the Porong Delta, as shown in Fig. 10. The simulated mangrove extent in Fig. 10b resembles the extent in the observed pattern in Fig. 10a obtained from integrating satellite and drone analysis from Beselly et al. (2021). The simulated mangrove extent tends to follow a similar shape as in Porong. However, the schematized model cannot reproduce a similar expansion rate as in the case study. The reasons can be explained as follows. First, we assume only single species in the model (*Avicennia* spp). Second, the northern delta lobe has multiple sources of propagules, i.e., from the northern mainland and the LUSI Island which can increase the number of individuals in the northern delta lobe. Third, in the absence of data for Porong, we assume that the reproduction rate is similar to that of *Avicennia germinans* (Grueters et al., 2014), even though reproduction is known to be species-specific. Forth, January–February is the peak of the rainy season. In this condition, the contribution of river discharge and local precipitation can contribute to longer-distance propagule transport from the multiple mangrove forests in the vicinity.

The canopy height trend of mangrove stands from the model shows a good agreement with the observation with an R^2 value of 0.982 and mean absolute error of 1.105 m (Fig. 10c). This value is compared to age-height relationship of the canopy height model from 2016 to 2021. Considering the simplified environmental forcing in the model and the variation of the environmental conditions in the case study, we expected a difference for each scenario but a similar trend.

3.2. *Mangrove response under seasonally changing environmental conditions*

3.2.1. *Response to salinity*

We found no direct effect of salinity on tree development in the low range chosen for the scenarios (0–25 ppt). No apparent difference exists between low and high salinity conditions in all scenarios, either in the canopy area or propagule production. This is due to the fact that *Avicennia* spp. are among the most salt-tolerant mangroves (Jayatissa et al., 2008) and will not be significantly affected until a salinity value of over 60 ppt is exceeded (Chen and Twilley, 1998).

We visually compare different salinity treatments (Hi Sal-Low Sal) within the same sediment load scenario (Table 1), i.e., the comparison of Hi Sal and Low Sal treatment for Rich Sed scenarios (A-C), Med Sed (B1-D1), and Poor Sed (B2-D2). We compare the effect of salinity on the canopy area (Fig. 8), on mangrove forest development for all sediment load scenarios (in Appendix 3), and propagule production (Fig. 11). Appendix 4 provides boxplots of monthly salinity values for each scenario. The effect of contrasting salinity conditions on the mangrove expansion pattern and the propagule production is relatively minor. The slightly larger mangrove extent in a lower salinity environment, as shown in Fig. 8, relates to how we parameterize low salinity by adding freshwater discharge during the dry season. Additional discharge from the river boundary during the dry season transported sediment, created more accommodation space, and thus increased the probability of seedlings being established. In addition, to clarify the argumentation, we devised all saline conditions of all Low Sal scenarios. These

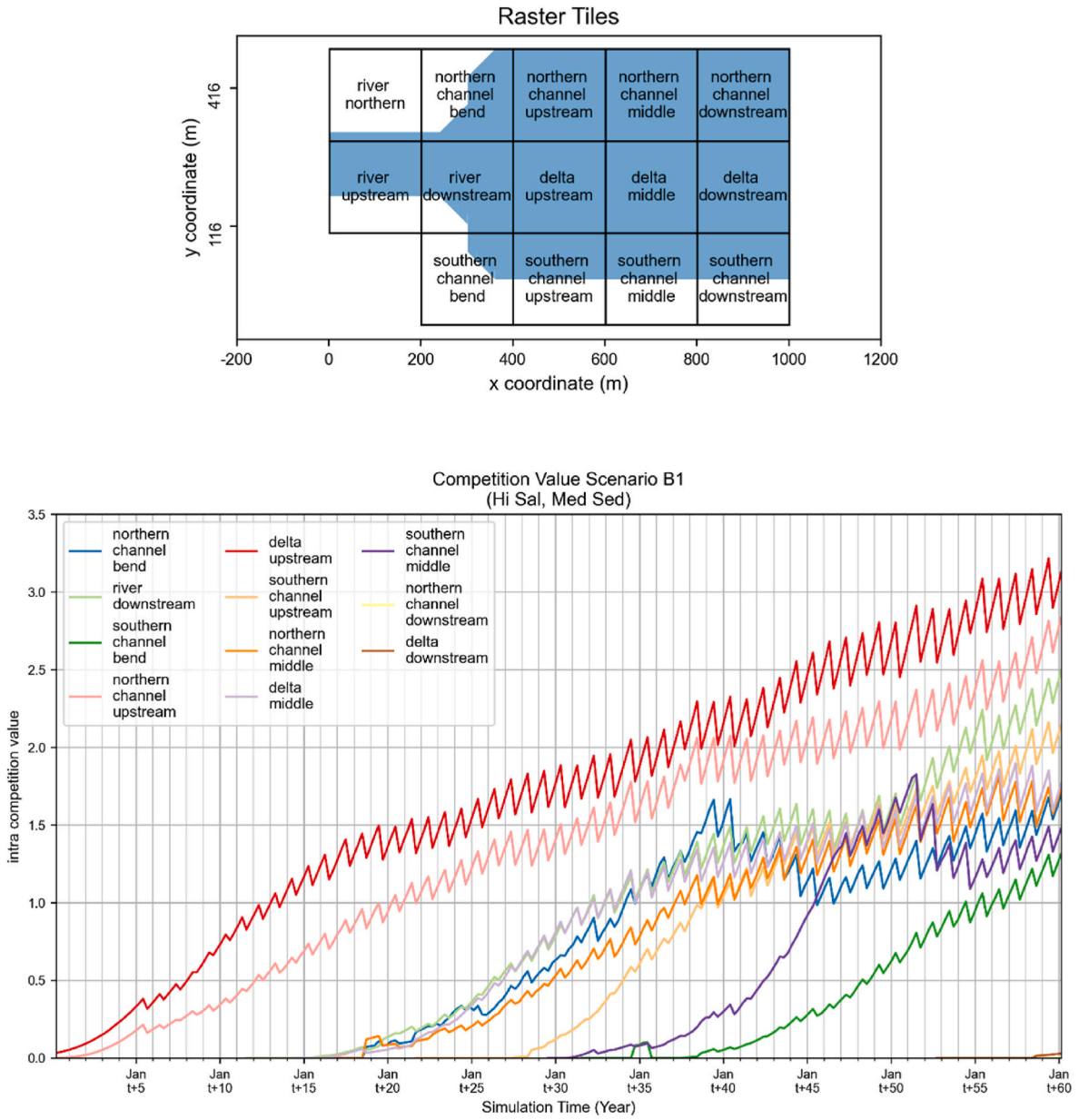

Fig. 9. The tiles of the MFON model (top panel) Intra-specific competition value (bottom panel) for each tile in Scenario A. Intra-specific competition value is averaged over each tile. The competition plot for all scenarios is provided in Supplement 2.

additional simulations would not represent real-world scenarios but rather allow us to test the pure effect of Low Saline compared to Full Saline conditions as opposed to the combined effect of salinity and high fresh-water discharged examined above. Results in Supplement 3 show that low salinity of 25 ppt makes a minor contribution to mangrove development, while sediment availability and the resulting accommodation space contribute more.

3.2.2. *Response to sediment availability*

Among the simulated physical drivers, sediment availability plays an important role in mangrove forest expansion (Rogers, 2021; Woodroffe et al., 2016; Xie et al., 2022). More sediment supply increases the accommodation space under accretive conditions. More accommodation space, in turn, increases the probability for the dispersed propagules to find space to settle and, in case the inundation period is low, to anchor the rooting system and develop. We compared the contrasting sediment conditions of the same saline environment, i.e., (Rich-Med-Poor Sed) with (Hi Sal): A-B1-B2, (Rich-Med-Poor Sed) with (Low Sal): C-D1-D2, and (Rich-Med Sed) with (Low Sal) and with (extra sediment in the dry season): E-F.

In Figs. 7 and 12, we observe rich sediment scenarios promoting the generation of a wider mudflat and, thus, more mangrove colonisation in a larger accommodation space, primarily visible in the streamwise or east-west cross-section (blue line). Looking at the panels, it is clear that the extent of the initial bed level (black line) is wide enough for the mangroves to expand. Sediment supply and fluvial discharge stimulated

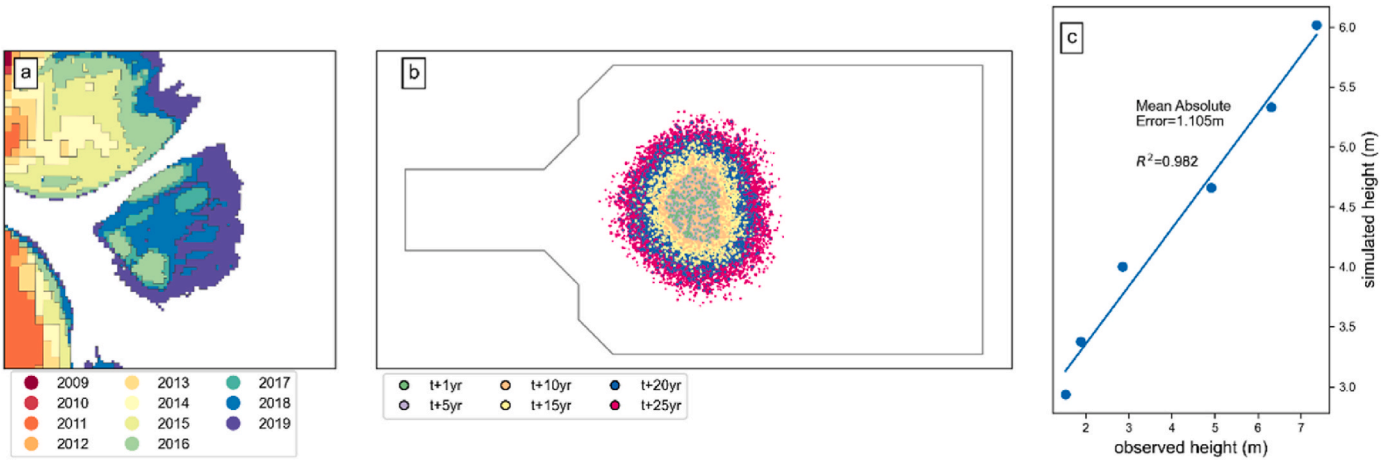

Fig. 10. Qualitative comparison of the DFMFON model with the Porong Delta (Indonesia) case study (Beselly et al., 2021). Beselly et al. produced an annual mangrove extent map (a) that reasonably matched the modelled development of mangrove extent in a schematized model domain (b) as well as the reasonable agreement of the observed and modelled height development (c).

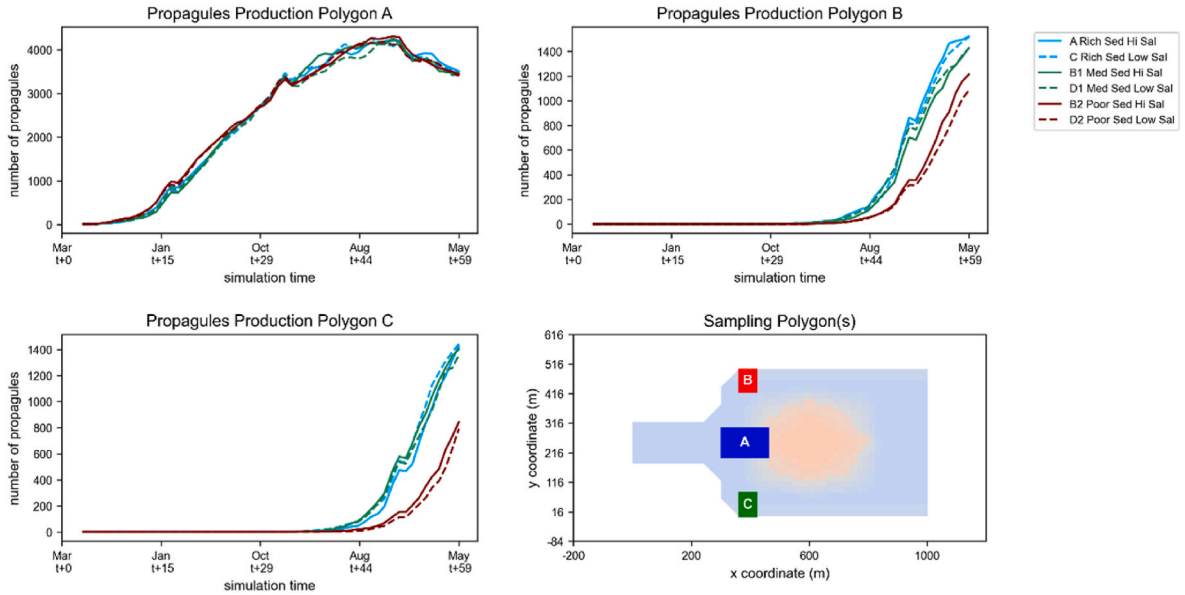

Fig. 11. Propagule production comparison plot for variation in salinity conditions. The figure compares the effect of salinity variation on propagule productions in similar sediment concentration environments. The surveyed polygons were carefully selected to ensure the minimal effect of changes in morphology by selecting the area with the lowest difference in cumulative erosion-sedimentation value. With this, we are confident the sampling polygons can represent different salinity treatments in the domain's main delta and northern-southern limit.

propagules in the delta to establish downstream. The flat and sufficiently high bed level increases the WoO and the establishment probability. Throughout the simulation period, the level of the riverbed changes slightly downstream. However, an upstream prograding pattern can be observed, where mudflat builds up, and mangroves establish. The outermost fringe of the mangrove is located at the edge of the mudflat on the line of the lowest low water level (LLWL).

Looking at the north-south cross-section, the dependence of mangrove establishment on bed level is more visible. In scenarios C and D1, a creek-like depression was created on the northward side of the mangrove forest after 23 years. However, since the depression was shallow enough, it was colonised by the mangroves. As an effect, this increased the bed level and widened the platform to the north and south. Therefore, more accommodation space was available, and thus, mangroves occupied the space until the LLWL line. We can also see the establishment due to propagule dispersal in the northern and southern limits of the domain, where accommodation space was available. It is more visible in scenario D2; until year 23, the bed level was lower, and no mangroves could establish. However, beginning with the year 41, the bed level was higher, and therefore, it could be occupied by the propagules and established seedlings. The contribution of belowground biomass is visible in all the plots, especially in the interior, even though minimal, in the order of millimetres annually.

3.2.3. *Seasonality*

To isolate the seasonality effect from the long-term trend, we decomposed mangrove area development at quarterly intervals (90 days) using LOESS analysis. Fig. 13 illustrates the decomposition into the mangrove area trend and seasonal components of Scenario A. Other scenarios show a similar component pattern in Supplement 4.

The seasonal component demonstrates that the development of the mangrove area follows an oscillating pattern mirroring the seasonal boundary conditions. A similar seasonality pattern of mangrove expansion (wet-dry season) was observed in the Porong Delta (Beselly

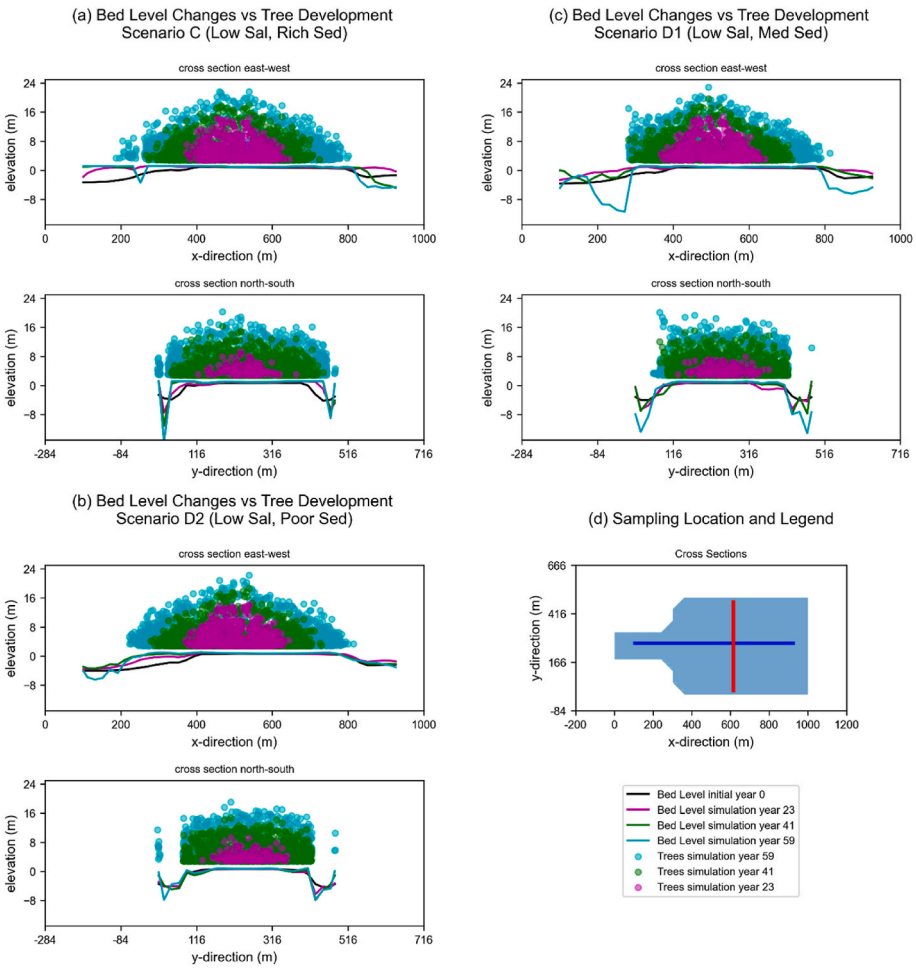

Fig. 12. The plot of mangrove forest development for scenario C (panel a), scenario D1 (panel b), scenario D2 (panel c), and the cross-section(s) on panel d. The plot shows the time series development of bed level and trees 23, 41, and 59 years after initialisation.

et al., 2021). Spatially, the extent of the variation is similar across the scenarios, ranging from $+500$ m^2 to -500 m^2. Temporally, within one year of simulation, one can observe growth during the wet season and decline during the dry season with an overall positive net rate.

In the seasonal variation panel of Fig. 13, we observe a wet-dry season cycle of mangrove dynamics. Mangroves expand in January, concurrent with the beginning of the propagules production. The mangroves are growing optimally during the wet season, given the river's freshwater discharge and high sediment supply. At the end of the wet season, the young mangroves maintain growth, profiting from low competition for the space provided by the sediment deposition and the relatively lower salinity associated with the wet season. This favourable environment prevails until September, which is in the middle of the dry season. The peak of mangrove expansion is in September, given the optimal conditions inherited from the wet season. After this peak, competition stress increases (Fig. 9) as the environment becomes less favourable due to low sediment availability and reduced bed level. The smaller (younger) trees die first while neighbouring trees develop less. The decrease in the mangrove area indicates that this process continues until January, when the cycle starts again with propagule production.

Residual or remainder represents noise in the data, where a residual of 0 means that seasonal and trend components well represent the time series. Four relatively high residuals are present in the lower panel of Fig. 13. We associated those with the breakpoints that separated the three phases of mangrove area development as described in section 3.1. The first breakpoint occurred after five years of development; it marks the beginning of the phase when the initial population has matured, and the first generation of seedlings is recruited. The second breakpoint occurred after about 15 years and is associated with the onset of phase 2 when mature populations occupied the middle delta and produced more propagules. As the mudflat was wide enough and the WoO probability was high, the transported propagules occupied the space and were established. The third breakpoint occurred 30 years after initialisation; it is associated with the beginning of phase 3, in which the northern and the southern channel were occupied by propagules originating from parental trees of the middle delta. As the northern and southern channel populations grew, they started their reproduction phase at breakpoint 4.

3.2.4. *Mangrove stand structure*

Fig. 14b shows histograms of tree number-height distributions as indicators of the stand structure sampled on various rectangular plots (Fig. 14a) over time. The pattern of all scenarios is almost identical. Therefore, we have chosen Scenario A as a representative to describe the stand structure. We sampled the tree structure in four polygons. Polygon A represents the delta forest with the centre point taken from the initial trees with a size of 100 $\times$ 100 m and Polygon B with a size of 300 $\times$ 300 m. Polygon C is sized 100 $\times$ 100 m and is located upstream with the same latitude as Polygon A and B. The decision to put Polygon C upstream is to explore whether the younger population in C, in comparison to the population in A and B, exhibits a different pattern. Polygon D has a size of 100 $\times$ 300 m, located at the fringe of the main delta and channel. We provide comparative stand structure plots at 5-year intervals to represent the three major phases as in section 3.1. Hence, 12 plots are made available for each polygon. The complete plots for all sampling

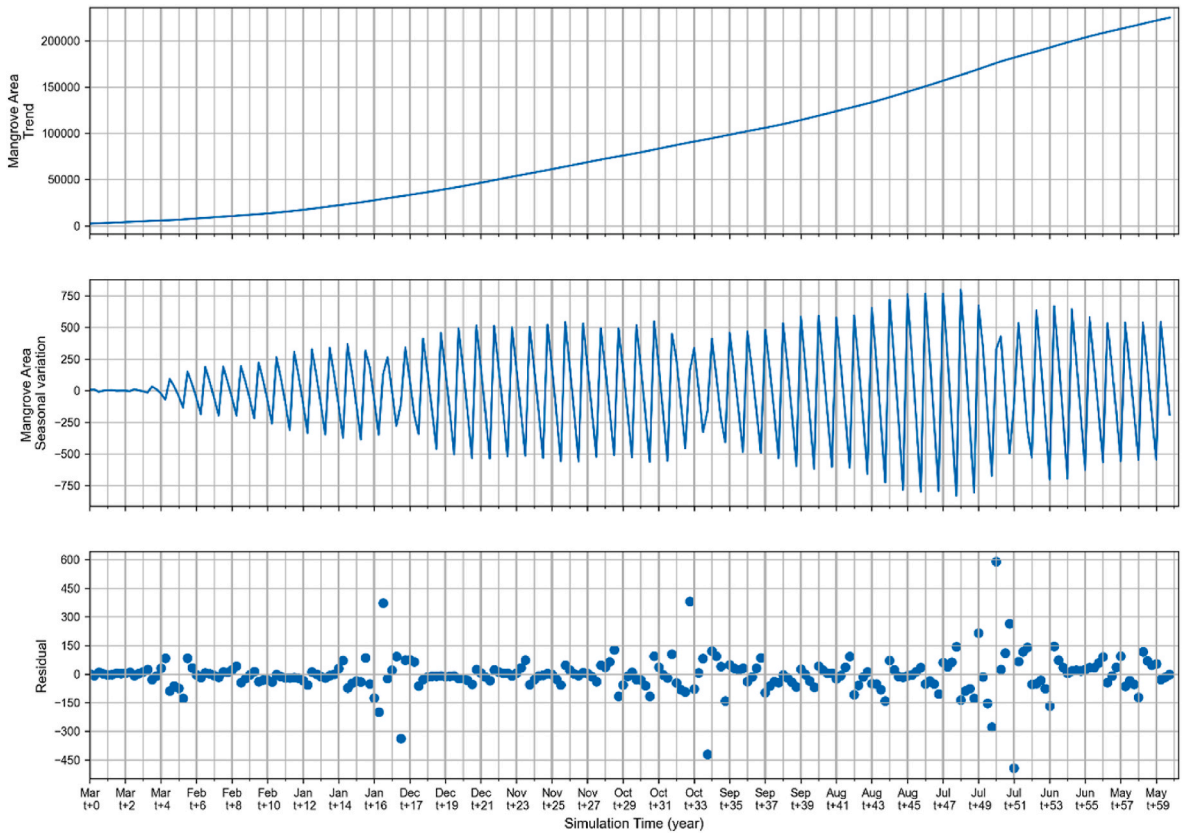

Fig. 13. Temporal decomposition with LOESS for scenario A. Here in the plot, we decompose the seasonal variation of the mangrove area (m^2) to the trend (above panel), seasonal variation (middle panel), and residual component (lowest panel).

polygons and other scenarios are provided in Supplement 5.

The histograms show a slight or almost flat decline with increasing height (in cm) in the first 20 years of the simulations. Year 0 shows the height class distribution of the initial trees. After five years, we see 2 bars with the initial trees that matured on the right bar and the distribution of young trees on the left bar. Year 10 and year 15 represent the stand structure of young mangrove populations where the number of parental trees limits the sapling population. Given the space availability, most of the younger trees in year 10 survive to year 15. From the age of 20 years, mangrove stands become older with a higher density. This corresponds to the increasing propagule production. Despite the larger number of new saplings, with competition, younger trees died first since their FONs overlapped with the larger FONs of older trees due to their higher density. It is clearly seen by the constant distribution of older trees that they survived to the next observation period.

Comparing polygons A and B, both have a similar pattern. However, since Polygon B includes the fringe area, the fraction of younger trees in the population is higher. Polygon A contains fewer saplings since it has an older population, larger height, larger diameter at breast height (dbh), and thus lower density. Polygons C and D are located in the fringing area. Therefore, they both have lower sapling density than A and B. A prevalence of the younger individuals and a high expansion capacity are typical characteristics of fringing mangroves.

3.3. Hydro-morphodynamic evolution of the deltaic mangrove

In this section, we explore the impacts of mangroves on morphological evolution and hydrodynamics.

3.3.1. Influence of mangroves on hydrodynamics

The differences in hydrodynamics between simulations, including and excluding mangroves, are mainly due to the role of mangrove-induced drag and turbulence, which alters the magnitude and direction of the flow. Fig. 15 illustrates how the presence of mangroves alters hydrodynamics. We capture the strength and direction of currents as patches-and-vector plots for Scenario E. The ebb tide exhibits the largest flow velocities because of the combined effect of tide and river flow. The simulation is year 56, meaning that the mangrove population in the delta is in a dense, mature state, and the population has colonised the northern and southern parts. When the vegetated area becomes inundated, an additional drag by the mangroves reduces the strength of the current to almost 0 m/s. In comparison, excluding mangroves in the same area with the same bathymetry yields a larger value between 0.05 and 0.1 m/s. A difference in magnitude is detailed in Fig. 15c. The extra resistance provided by the mangroves in the delta lobe and the northern-southern part resulted in a concentration of flow in the channels. Therefore, we observed a higher flow rate in both channels regardless of whether the simulation included or excluded mangroves.

3.3.2. Morphological evolution, with and without mangroves

The hydro-morphological model was first used to simulate the prograding delta development resulting from fluvial sediment supply including-excluding mangroves and to examine the effect of mangroves. As shown in Fig. 12 and section 3.2.2, sediment availability is an important physical driver limiting mangrove forests' lateral expansion. Low sediment concentrations of the Poor Sed scenarios do not gain as much surface level as the Rich Sed scenarios. Since mangroves require suitable habitat (accommodation space), the Poor Sed scenarios tended to contain smaller mangrove areas in comparison to Rich Sed conditions.

Fig. 16 compares bed level evolution for mangroves and no-mangroves simulations at four moments in time. The timestamps reflect the early dynamics (year 5), phase 1 (year 23), phase 2 (year 41), and approaching the end of the simulation (year 59). The effect of mangroves is clearly seen in the years 41 and 59. As the mangroves

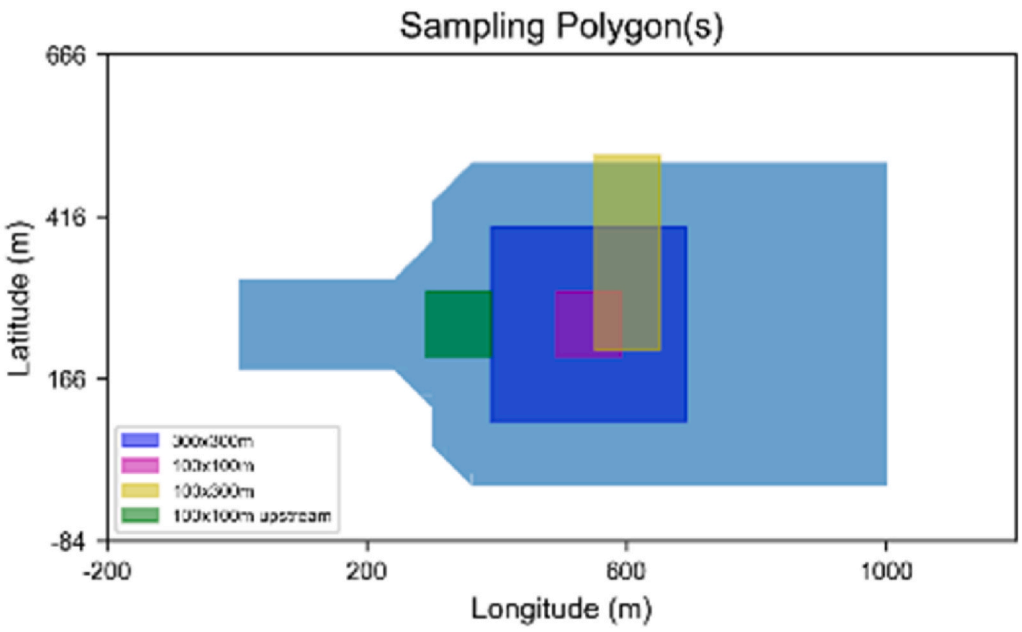

a.

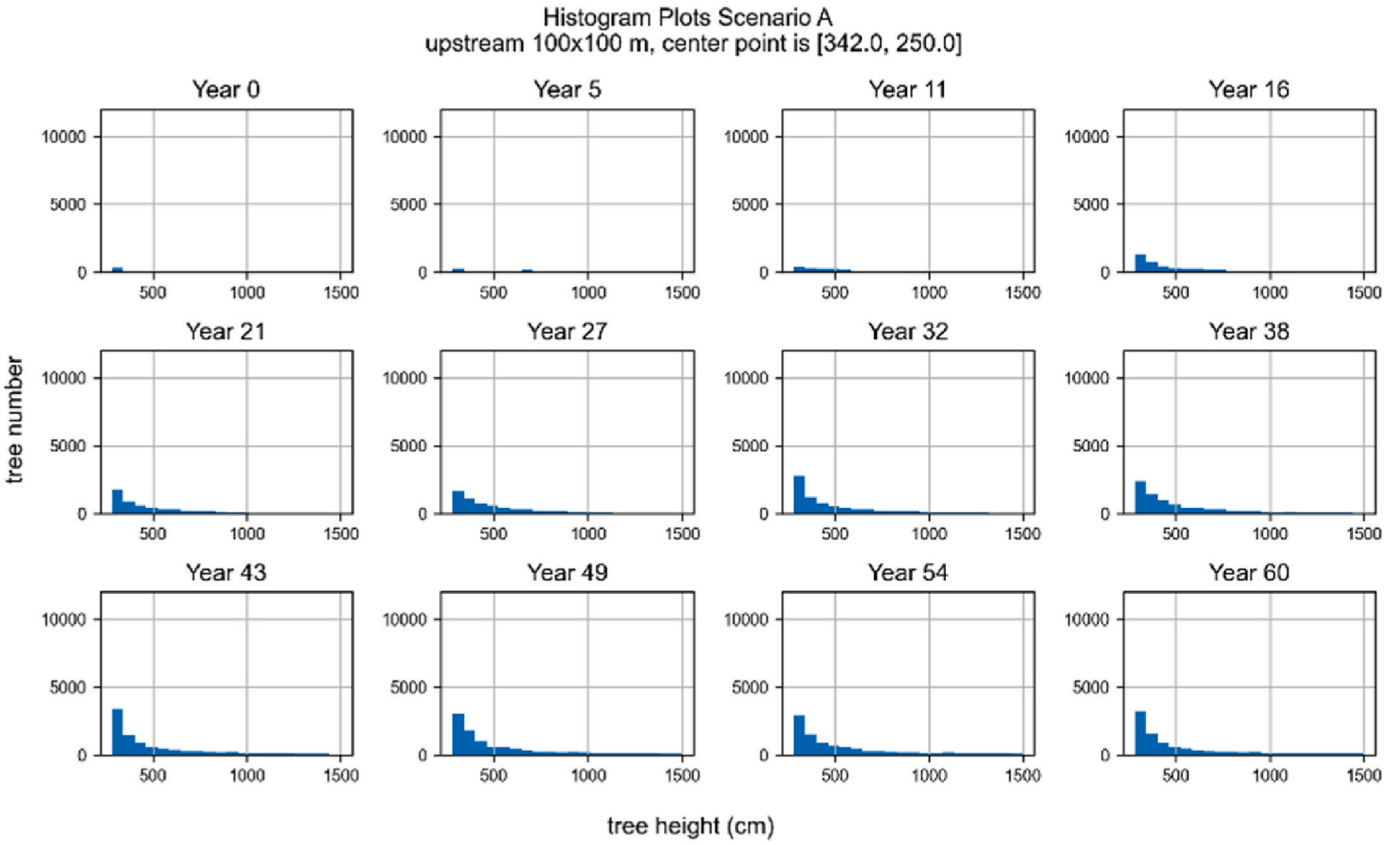

b.

Fig. 14. Tree number-height histograms on the selected polygons for Scenario A. Surveyed polygons (a), histogram of polygon 100 × 100 m (b), histogram of polygon 100 × 100 m in the upstream (c), histogram 100 × 300 m (d), and histogram of polygon 300 × 300 m (e). The histograms for other scenarios are provided in Supplement 5.

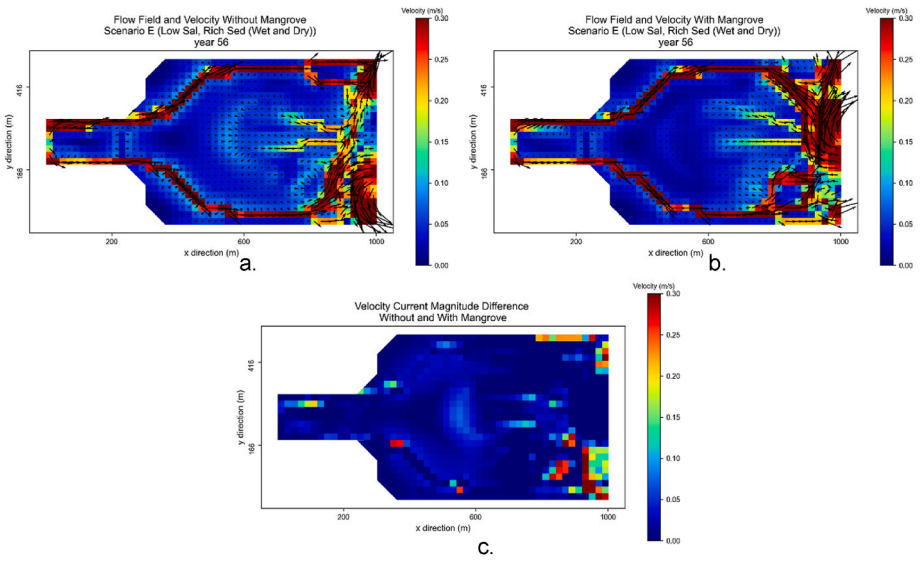

Fig. 15. Snapshot plot of the flow field and velocity for simulations (a) with- and (b) no-mangroves for Scenario E. The difference in current magnitude between excluding and including the mangrove scenario is presented in (c).

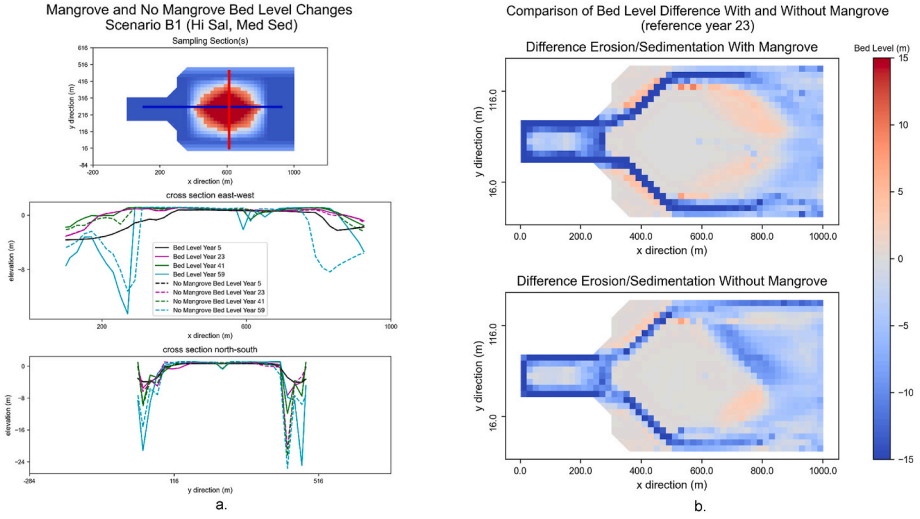

Fig. 16. (a) Bed level evolution in simulations with mangrove (full line curves) and without mangrove (dashed curves) for Scenario B1. The streamwise or east-west section is depicted as a blue line, whereas the crosswise or north-south section is depicted as a red line. (b) Bed level difference of no- and with-mangroves simulation at coupling 243 (year 60) with reference year 23 for Scenario B1. The complete set of bed-level difference plots for all scenarios is provided in Appendix 5.

individually grow larger and population-wise wider, they alter the hydrodynamics by increasing the bulk drag coefficient. Their presence promotes the deposition of freshly supplied sediment on the updrift and lee side of the delta. The streamwise plot shows it is more significant on the seaward side. The no-mangroves simulation faced considerable erosion.

Large bed level changes occurred (Fig. 16a) within the first five years due to deposition in the upstream part of the delta, the build-up of a new tidal flat downstream, and the deepening of the northern and southern channels. River discharge in the upstream boundary causes an accelerating current in the northern-southern channels and incises the bathymetry. The presence of a delta island at the bifurcation locally reduces the velocity-enhancing deposition. The downstream of the delta also experiences deposition because of decelerating flow due to the presence of dense forest. The tidal currents promote the formation of additional tidal flats with an elliptic-like shape at the lee side. In the first 15–20 years, the impact of mangroves on morphological development remains limited. It is because mangroves are still small and sparse and thus have limited effects on hydrodynamics. After this time, the impact of mangroves becomes larger, with some differences between scenarios.

Since sediment supply initially dominates the morphodynamics, we used the year 23-bed level as the reference for the following analysis

(Fig. 16b). Overall, simulations with-mangroves show more deposition in mangrove-colonised areas than simulations without mangroves, particularly in the northeastern part of the delta. Under no-mangroves conditions, the delta is incised by a northwest-southeast channel. In contrast, the with-mangroves condition leads to wider accommodation space in the delta and higher bed levels in the northern and southern parts of the channel. In a condition where the mangrove stand structure is wide and dense and located in a sediment-rich environment, it is likely that mangroves could act as ecosystem engineers. In this sense, the forest has the capacity to build its own environment by slowing down the current and building up the mudflat on the lee side. When the inundation regime favours mangrove establishment, mangroves opportunistically occupy the new mudflat. Where the accommodation space is abundant and the population is relatively small, for instance, in sediment-rich conditions and with more accommodation space, the mangroves are likely to be opportunistic. In this study, the mangrove dynamics of the first 15–20 years were characterized by the opportunistic-colonizer behaviour of the mangroves, filling the accommodation space.

4. Discussion

4.1. Interplay of the physical, environment, and mangrove dynamics

The DFMFON model has been developed to address the challenge of understanding how mangroves respond to changes in the physical environment and how the dynamic response of mangroves feeds back to the physical environment. Our study advances the currently segregated knowledge by coupling an individual-based mangrove model with a mechanistic hydro-morphodynamic model. To the best of our knowledge, this is the first modelling study that explicitly solves the question of how a mangrove population responds in terms of stand structure and tree sizes to the hydro-morphodynamic drivers and salinity variability. This is considered an important advance, for instance, to meet an increasing necessity in predicting the mangrove forest structure trajectory in detailed physical-environmental scenarios (Dahdouh-Guebas et al., 2022; Twilley and Rivera-Monroy, 2005).

Our coupled DFMFON model satisfactorily elucidates the intertwined role of physical drivers (hydromorphodynamics), environmental drivers (salinity), and mangroves on a seasonal basis. Based on the physical characteristics of the Porong Delta, the schematized 2DH model simulations can reproduce the realistic spatiotemporal variation of mangrove dynamics on a sediment-rich system. Our study shows how the feedback effect of mangroves on the physical-environmental drivers leads to alternating expansion and contraction of mangrove extent instead of linear growth (Alongi, 2008; Krauss et al., 2014; McKee, 2011; Rogers, 2021).

Our numerical experiments unravel the dependency of the mangrove ecosystem on the available accommodation space. Evidence of this is the influence of the prograding mudflat platform on seaward mangrove expansion (Rogers, 2021; Woodroffe et al., 2016) and the influence of flow velocity on propagule dispersal. The presence of mangrove stands provides positive morphological feedback by the additional flow resistance. It promotes the mudflat build-up downstream (as also reported by Furukawa and Wolanski, 1996), provided that the stands are mature, dense enough and are situated in the direction of the dominant current. The interactions vary through space and time; hydrodynamic patterns are primarily influenced by the local topography through the first 15 years or phase 1 and mangrove-induced in phases 2 and 3 when the population reaches its maturity (Figs. 7, Figure 8, and Fig. 13). The hydrodynamic conditions are temporally varying when subjected to the spatiotemporal changes in forest structure since the hydrodynamic is dependent on mangrove biophysical properties (Maza et al., 2021). Therefore, we observed the difference in mangrove response (with mangrove canopy area as a proxy) to the stressors at several breakpoints in time. Mangroves play a limited role in morphological changes during the first 20 years as their low and less dense structure has a limited impact on hydrodynamics (Fig. 16), shown by the little difference in bed level between scenarios with and without mangroves. When the mangrove forest has grown mature enough and achieved sufficient structure, its presence is relevant in adding hydrodynamic resistance and, thus, helps to promote the build-up of the mudflat platform. It can be argued that the transition from mangroves acting as colonizers to mangroves functioning as ecosystem engineers occur when mangroves are mature, tall, and structurally dense enough. Thus, in this state, environmental variation has little effect on growth. When accommodation space is available, the mangroves shift to colonisers by dispersing their propagules. At the same time, the ecosystem engineer function maintains the resilience of the recently recruited seedlings through their innate tree-to-tree competition. These processes will eventually result in the optimal number of established trees after the stand has reached the self-thinning line depending on the habitat conditions.

Mangroves' vertical growth and lateral expansion depend on physical drivers and competition. Simulation results provide little correlation between the variability of mangrove dynamics and the seasonal variation of environmental stressors (Figs. 9 and 13). Even though bed level accretion due to sediment availability is the dominant factor, hydrodynamic condition plays a role in dispersing the propagules during the propagule production season, contributing to the resilience of the forest (Dahdouh-Guebas et al., 2022; Shih et al., 2022). The contribution of salinity is rather minor considering low salinity variation and *A. marina* as among the most salt-tolerant mangrove species. The net development of the mangrove forest is a product of seasonal variation, being lowest after the more stressful conditions in the dry season. The abundant fresh water and fluvial sediment fluxes at the beginning of the wet season help mangroves rejuvenate and distribute the propagules in their vicinity. The positive trend continues until the middle of the dry season. The stressful environment then adds to competition, hinders growth, and increases mortality, particularly among juveniles. The capability to model seasonality, as in our work, is important for understanding the phenological response of mangroves to stressors, which determines the dynamics and productivity (Sharma et al., 2014; Zhang et al., 2016). Several studies demonstrate the mangroves' response to substantial seasonal fluctuation, e.g., of temperature (Duke, 1990), light (Suwa and Hagihara, 2008), precipitation (Duke et al., 1984), nutrient (Lagomasino et al., 2014), freshwater and hydroperiod (Kamruzzaman et al., 2013; Slim et al., 1996; Wafar et al., 1997).

4.2. Model limitations, potential uses, and future research needs

The development of this DFMFON-coupled model is intended as a design tool to quantify the functionality and persistence of the mangrove ecosystem as coastal protection that is currently lacking (Dahdouh-Guebas et al., 2022; Ellison et al., 2020; Schoonees et al., 2019). Therefore, parameterisation of physical-environmental drivers has been chosen to describe the main relationships between mangroves and changes in physical processes and vice versa. We decided to consider only salinity as the main environmental driver that controls mangrove growth (Sudhir et al., 2022), without feedback from mangroves on salinity distribution due to freshwater uptake (Bathmann et al., 2020). Besides salinity, we assume favourable environmental conditions that cause no biotic damage to mangroves, as presented in Fig. 17. The main underlying assumption in terms of tree growth, competition, and salinity tolerance is that *A. marina* behaves like *A. germinans, except for* propagule production, which resembles that of *A. marina* in Porong Forest, and WoO parameterisation based on those measured by Balke et al. (2015) in the Firth of Thames, New Zealand. Mangrove growth and mortality are indeed a complex processes. The environmental drivers provide the resources and regulators for tree diameter and height growth, while physical drivers limit the lateral expansion of the mangrove stand. With DFMFON, we explicitly determine the productivity of the mangrove based on the complete feedback loop of the physical drivers (water level,

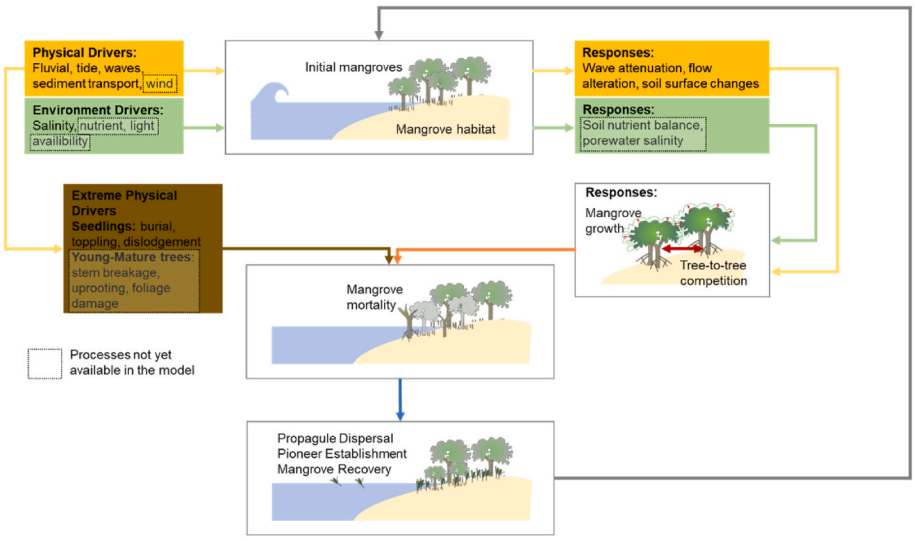

Fig. 17. Simplified overview of mangroves' relevant processes and interactions and the physical-environmental drivers in the DFMFON model.

flow, and bed level) and the influence of environmental drivers (salinity).

Mangrove establishment and propagule dispersal are the critical elements in assessing the persistence of mangrove forests (Van der Stocken et al., 2019). Estimating how a forest recovers after a large, infrequent disturbance such as a tropical storm is still a challenge. Current approaches use long remote sensing observations from other locations in the vicinity of the impacted forest (Krauss and Osland, 2019; Vizcaya--Martínez et al., 2022) to estimate the recovery time. The propagule distribution depends on the hydrodynamic condition, and the probability of the establishment is based on the WoO value. This contribution will be beneficial to fill the gap in simulated mangrove dynamics by incorporating the complete life cycle of mangroves and by considering physical processes in the model. Currently, our model only considers seedling-based regeneration and cannot model the re-sprouting mechanism (Krauss and Osland, 2019). We assume that the dispersal and settling of propagules only occur for a short period of time, i.e., two weeks after release (Section 2.1.4.3), taking into account the propagules' availability, travel time, and the obligate dispersal.

Competition and environment, in combination, are the main factors determining the mortality of saplings and mature trees alike. The WoO approach is used in the model to simulate the mortality during the propagule and seedling stage. The model does not include mechanical tree damage. For instance, exposure to extreme wind and waves during storm surges can break stems or uproot trees. Including mangroves' resistance to such exposure in the model should be relevant when considering the function of coastal protection (Morris et al., 2019; World Bank, 2017). Several mechanistic models can estimate tree breakage, e.g., HWIND and GALES (Gardiner et al., 2008) and individual branches mechanical tests (van Hespen et al., 2021). However, HWIND and GALES models have been applied for even-aged forest plantations, while the mechanical test focused more on individual trees. Additionally, the mortality threshold for mangroves for such breakage mechanisms is not yet known.

The model has shown that it can reliably replicate mangrove forest expansion. It has deepened the mechanistic understanding of large-scale and long-term mangrove forest expansion behaviour in different detailed environment scenarios. Development of this model may lead towards improved prediction of changes in mangrove forest structure and species composition (Aslan et al., 2016; Ellison et al., 2022) due to climate change and anthropogenic activities. An increase in economic activities is sometimes identified as the main driver of mangrove forest conversion to shrimp farms, rice agriculture, oil palm plantations, or construction projects (Jayanthi et al., 2022; Richards and Friess, 2016). These kinds of activities could result in habitat segregation, where the interconnectedness with ecosystems in the vicinity is important for, e.g., nutrient exchange and, in the end, could lead to the collapse of the mangrove ecosystem (Curnick et al., 2019). Since little is known about mangrove fragmentation and disconnectivity (Dahdouh-Guebas et al., 2022), we can apply the model to investigate the sensitivity of mangrove forest persistence capacity to the loss rate of mangrove patches, their shape, size, and distance. Apart from local topography and prevailing storm intensities, structural characteristics of mangrove forests, such as species composition, tree height, and density, are important parameters for assessing their capability to provide nature-based coastal protection. We could extend the DFMFON model with a wave model to investigate the sensitivity of mangrove wave attenuation to spatiotemporal changes in forest structure and composition (Maza et al., 2021).

5. Conclusions

In our study, a mechanistic simulation model that captures the interrelationships of individual tree responses and the changing environment was created by coupling the DFM and MFON models. To our knowledge, our novel eco-morphodynamic model is the first that offers to examine the sensitivity of mangrove forest structure to changes in hydrodynamics (water level and current), morphology (bed level), and salinity in a feedback loop. The model demonstrates the seasonal variation in mangrove dynamics and is the first to account for the interactions between mangroves and stressors at all life stages from propagule to seedling ($\leq$1.37 m and $\geq$1.37 m), sapling, and mature stages, including short/long distance propagule dispersal. This gives an advantage to mechanistically model forest expansion, retreat, and colonisation influenced by physical-environmental drivers. The simulations were initialized in a schematized delta setting with a small patch of saplings and seasonal fluvial forcing. When the stand is young and sparse, the mangrove forest has a modest effect on morphology, and the bed-level development with vegetation is quite similar to the scenario

without vegetation. As long as accommodation space is available, the mangrove population tends to occupy the space within its physical drivers limit. In contrast, mature and dense mangrove populations are likely capable of altering their habitat by promoting the deposition in the direction of the dominant current. Overall, the model exercise presented here highlights the benefit of integrating an individual-based mangrove and a hydromorphodynamic model in providing a mechanistic understanding regarding the feedback loop of physical-environmental drivers and changes in mangrove forest structure over space and time.

Funding

This research is funded by LPDP with grant number 201710220111567.

Declaration of competing interest

The authors declare the following financial interests/personal relationships which may be considered as potential competing interests: Sebrian Mirdeklis Beselly Putra reports financial support, equipment, drugs, or supplies, and travel were provided by Indonesia Endowment Fund for Education.

Data availability

The codes and data used in the research are available in the first author's GitHub repository as provided in the manuscript.

Software availability

Software name: DFMFON Mangrove-Morphodynamic Model
Developer: Sebrian Mirdeklis Beselly Putra
Contact address: s.besellyputra@un-ihe.org; sebrian@ub.ac.id
Year first official release: 2023
Hardware requirements: PC
System requirements: Windows
Software required: Delft3D-Flexible Mesh and MesoFON
Program language: Python
Program size: DFMFON (source code) 400KB / 100MB with example;
Delft3D-FM (compiled) 1.06GB, see https://svn.oss.deltares.nl/;
MesoFON (executable Java jar file) 67MB, see http://mesofon.org and https://github.com/grueters/MesoFON
Availability: https://github.com/smbeselly/DFMFON
License: GPL-3.0 license
Documentation: README in Github repository

Appendix 1. DFM Model Parameters

Parameter	Value	Unit	Remarks
Domain	2500 × 500	[m]	Porong Delta
Cell Size	20 × 20	[m]	
Model Time Span	60	[years]	
Hydrodynamic Time Step	200	[s]	DtUser
Morphological Factor	30	–	MorFac
Sediment Type	Mud	–	SedTyp
Reference Density for hindered settling	1600	[kg/m^3]	Cref
Specific Density	2650	[kg/m^3]	RhoSol
Dry Bed Density	500	[kg/m^3]	CDryB
Fresh Settling Velocity	0.005	[m/s]	WS0
Saline Settling Velocity	0.005	[m/s]	WSM
Critical Bed Shear Stress, Sedimentation	1000	[N/m^2]	TcrSed
Critical Bed Shear Stress, Erosion	0.3	[N/m^2]	TcrEro
Erosion Parameter	5.0 × 10^5	[kg/m^2/s]	EroPar
Initial Sediment Layer Thickness at Bed	30	[m]	IniSedThick
Spin-up Interval	540	[s]	

Appendix 2

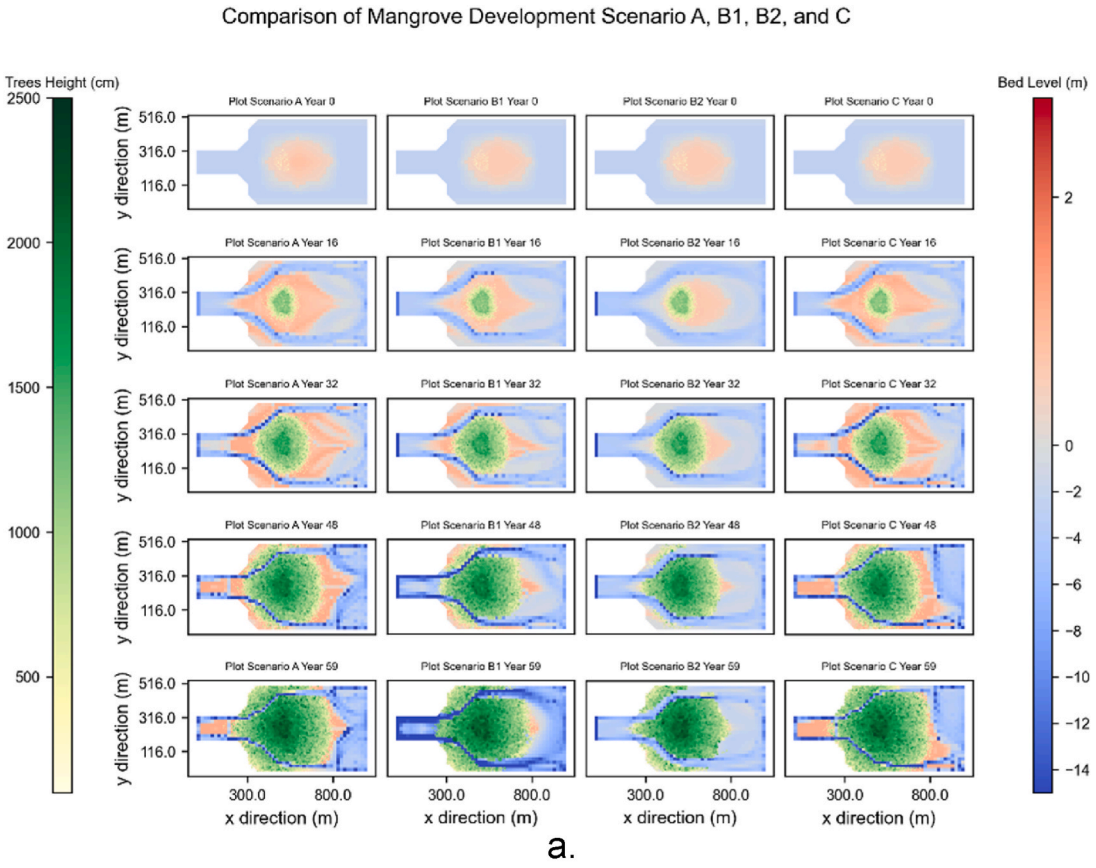

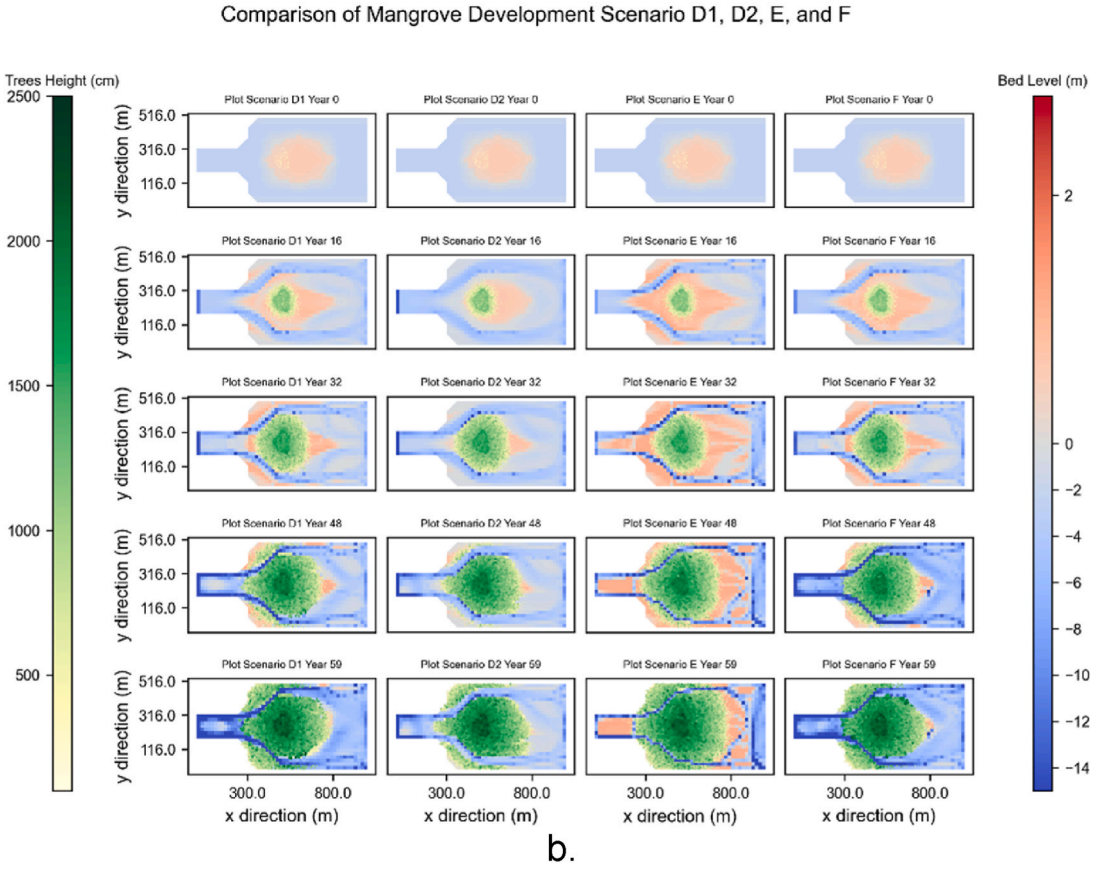

Figure A.1. Plot of the mangrove development for all scenarios. Scenario A (Hi Sal, Rich Sed), B1 (Hi Sal, Med Sed), B2 (Hi Sal, Poor Sed), and C (Low Sal, Rich Sed) in panel a and scenario D1 (Low Sal, Med Sed), D2 (Low Sal, Poor Sed), E (Low Sal, Rich Sed [Wet and Dry]), and F (Low Sal, Med Sed [Wet and Dry]) in panel b.

Appendix 3

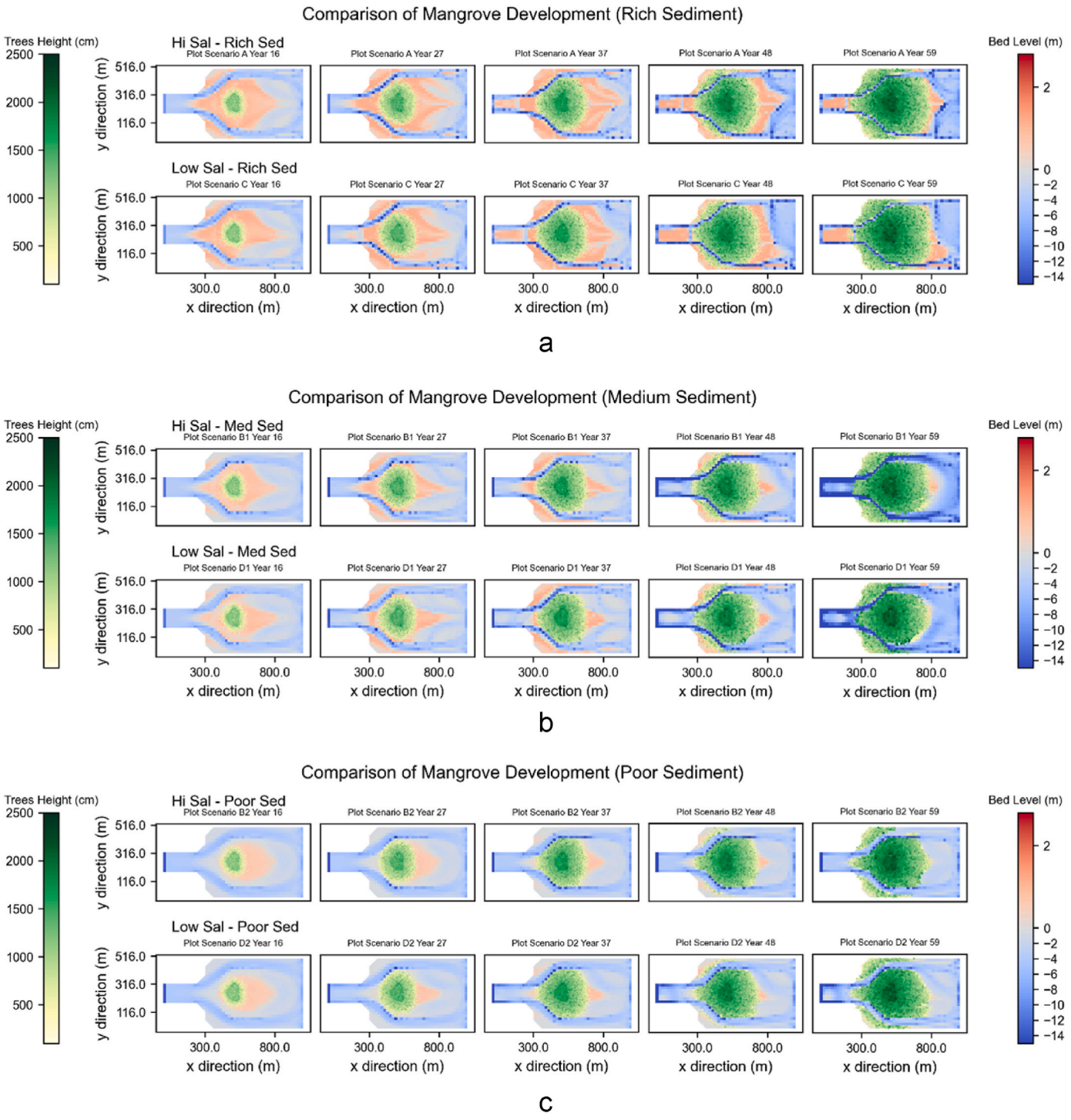

Figure A.2. Comparison of the effect of salinity to mangrove dynamics. The three panels show contrasting simulation results of the contrasting salinity environment on the same availability condition.

Appendix 4

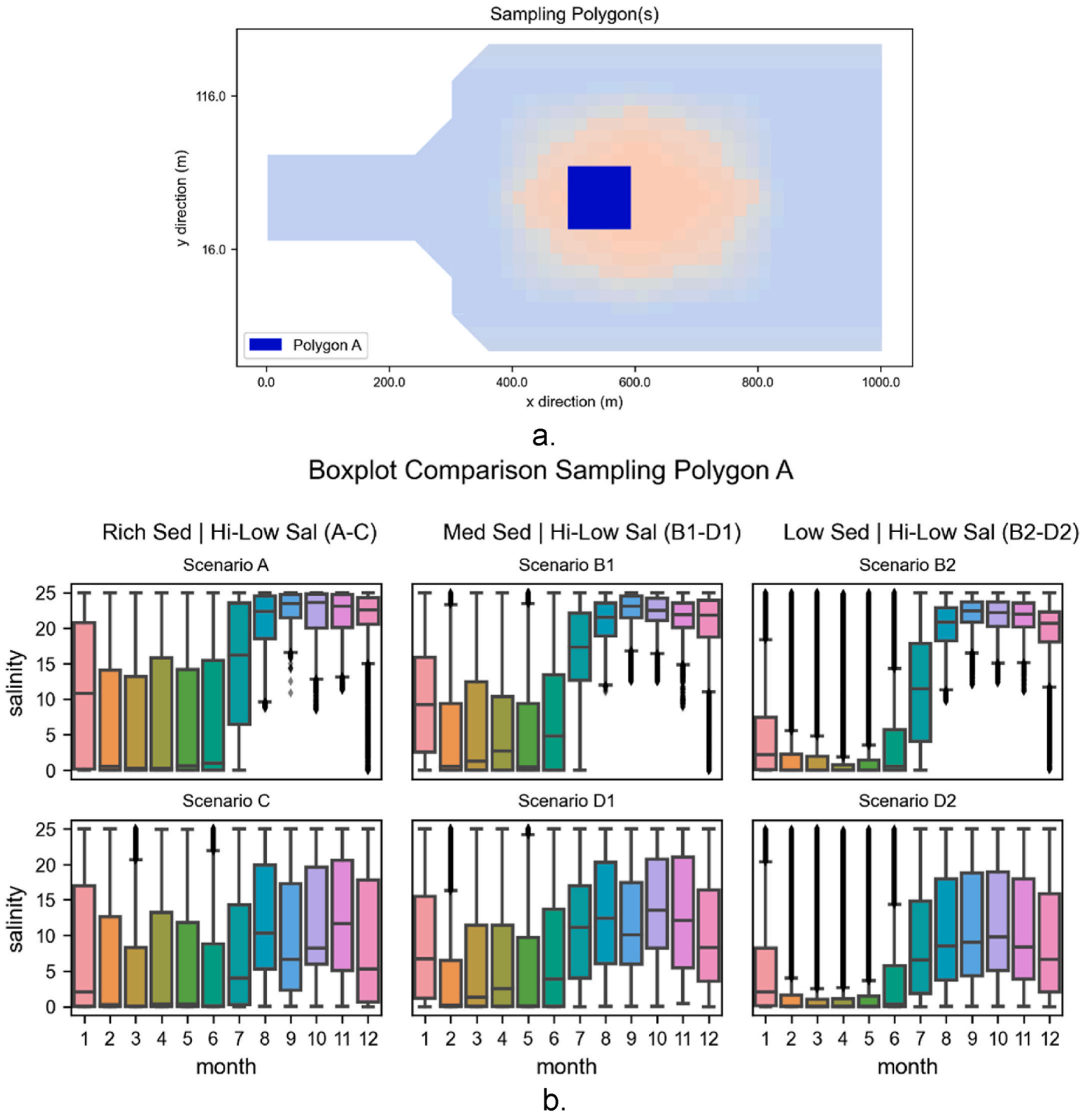

Figure A.3. Boxplot of simulated salinity sampled on Polygon A. Monthly variation of salinity value on Polygon A for different salinity conditions. the boxplot is arranged vertically, where similar sediment concentration is in the same column, with high salinity condition above the low salinity plot.

Appendix 5

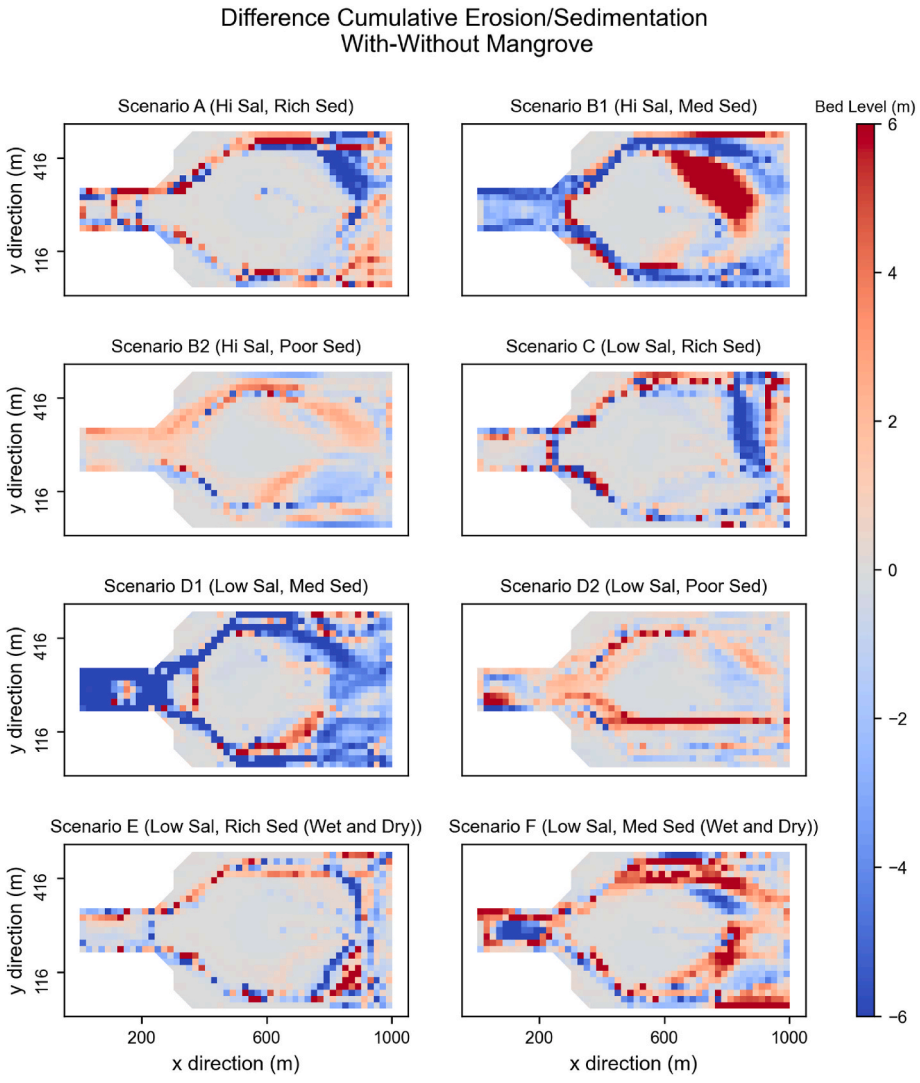

Figure A.4. Delta difference cumulative of bed level from with and without mangrove with cumulative erosion/sediment is calculated with the reference of year 23 as in section 3.3.2.

Appendix A. Supplementary data

Supplementary data to this article can be found online at https://doi.org/10.1016/j.envsoft.2023.105814.

References

Allen, J.A., Krauss, K.W., 2006. Influence of propagule flotation longevity and light availability on establishment of introduced mangrove species in Hawai'i. Pac. Sci. 60, 367–376. https://doi.org/10.1353/psc.2006.0015.

Almahasheer, H., Duarte, C.M., Irigoien, X., 2016. Phenology and growth dynamics of Avicennia marina in the central red sea. Sci. Rep. 6, 37785 https://doi.org/10.1038/srep37785.

Alongi, D.M., 2008. Mangrove forests: resilience, protection from tsunamis, and responses to global climate change. Estuar. Coast Shelf Sci. 76, 1–13. https://doi.org/10.1016/j.ecss.2007.08.024.

Anwar, C., 2006. Prediksi musim buah empat jenis mangrove berdasar hasil fenologinya. J. Penelit. Hutan Dan Konserv. Alam 3, 237–247. https://doi.org/10.20886/jphka.2006.3.3.237-247.

Anwar, C., Gunawan, H., 2006. Peranan ekologis dan sosial ekonomis hutan mangrove dalam mendukung pembangunan wilayah pesisir. Presented at the. In: Prosiding Ekspose Hasil-Hasil Penelitian. Konservasi dan Rehabilitasi Sumberdaya Hutan, Departemen Kehutanan Badan Penelitian dan Pengembangan Kehutanan Pusat Penelitian dan Pengembangan Hutan dan Konservasi Alam, Padang, p. 316.

Aslan, A., Rahman, A.F., Warren, M.W., Robeson, S.M., 2016. Mapping spatial distribution and biomass of coastal wetland vegetation in Indonesian Papua by combining active and passive remotely sensed data. Remote Sens. Environ. 183, 65–81. https://doi.org/10.1016/j.rse.2016.04.026.

Balke, T., Bouma, T., Horstman, E., Webb, E., Erftemeijer, P., Herman, P., 2011. Windows of opportunity: thresholds to mangrove seedling establishment on tidal flats. Mar. Ecol. Prog. Ser. 440, 1–9. https://doi.org/10.3354/meps09364.

Balke, T., Swales, A., Lovelock, C.E., Herman, P.M.J., Bouma, T.J., 2015. Limits to seaward expansion of mangroves: translating physical disturbance mechanisms into seedling survival gradients. J. Exp. Mar. Biol. Ecol. 467, 16–25. https://doi.org/10.1016/j.jembe.2015.02.015.

Baptist, M.J., Babovic, V., Rodríguez Uthurburu, J., Keijzer, M., Uittenbogaard, R.E., Mynett, A., Verwey, A., 2007. On inducing equations for vegetation resistance. J. Hydraul. Res. 45, 435–450. https://doi.org/10.1080/00221686.2007.9521778.

Barbier, E.B., Koch, E.W., Silliman, B.R., Hacker, S.D., Wolanski, E., Primavera, J., Granek, E.F., Polasky, S., Aswani, S., Cramer, L.A., Stoms, D.M., Kennedy, C.J., Bael, D., Kappel, C.V., Perillo, G.M.E., Reed, D.J., 2008. Coastal ecosystem-based management with nonlinear ecological functions and values. Science 319, 321–323. https://doi.org/10.1126/science.1150349.

Bathmann, J., Peters, R., Naumov, D., Fischer, T., Berger, U., Walther, M., 2020. The MANgrove–GroundwAter feedback model (MANGA) – describing belowground competition based on first principles. Ecol. Model. 420, 108973 https://doi.org/10.1016/j.ecolmodel.2020.108973.

Berger, U., Hildenbrandt, H., 2000. A new approach to spatially explicit modelling of forest dynamics: spacing, ageing and neighbourhood competition of mangrove trees. Ecol. Model. 132, 287–302. https://doi.org/10.1016/S0304-3800(00)00298-2.

Beselly, S.M., van der Wegen, M., Grueters, U., Reyns, J., Dijkstra, J., Roelvink, D., 2021. Eleven years of mangrove–mudflat dynamics on the mud volcano-induced prograding delta in East Java, Indonesia: integrating UAV and satellite imagery. Rem. Sens. 13, 1084. https://doi.org/10.3390/rs13061084.

Booker, J., Keogh, B., Chu, D., Conner, J., Hooper, I., 1998. Reproduction strategies of mangroves [WWW Document] Reprod. Strateg. Mangroves. URL. https://www.nhmi.org/mangroves/rep.htm.

Borsje, B.W., van Wesenbeeck, B.K., Dekker, F., Paalvast, P., Bouma, T.J., van Katwijk, M.M., de Vries, M.B., 2011. How ecological engineering can serve in coastal protection. Ecol. Eng. 37, 113–122. https://doi.org/10.1016/j.ecoleng.2010.11.027.

Buffington, K.J., MacKenzie, R.A., Carr, J.A., Apwong, M., Krauss, K.W., Thorne, K.M., 2021. Mangrove species' response to sea-level rise across Pohnpei, Federated States OF Micronesia (Report No. 2021–1002). Open-File Report. Reston, VA. https://doi.org/10.3133/ofr20211002.

Chamberlain, D.A., Phinn, S.R., Possingham, H.P., 2021. Mangrove forest cover and phenology with landsat dense time series in central queensland, Australia. Rem. Sens. 13, 3032. https://doi.org/10.3390/rs13153032.

Chen, R., Twilley, R.R., 1998. A gap dynamic model of mangrove forest development along gradients of soil salinity and nutrient resources. J. Ecol. 86, 37–51. https://doi.org/10.1046/j.1365-2745.1998.00233.x.

Chen, Y., Li, Yan, Cai, T., Thompson, C., Li, Yi, 2016. A comparison of biohydrodynamic interaction within mangrove and saltmarsh boundaries: bio-Hydrodynamics within Mangrove and Saltmarsh Boundaries. Earth Surf. Process. Landforms 41, 1967–1979. https://doi.org/10.1002/esp.3964.

Cheong, S.-M., Silliman, B., Wong, P.P., van Wesenbeeck, B., Kim, C.-K., Guannel, G., 2013. Coastal adaptation with ecological engineering. Nat. Clim. Change 3, 787–791. https://doi.org/10.1038/nclimate1854.

Clarke, P.J., 1993. Dispersal of grey mangrove (Avicennia marina) propagules in southeastern Australia. Aquat. Bot. 45, 195–204. https://doi.org/10.1016/0304-3770(93)90021-N.

Clarke, P.J., Kerrigan, R.A., Westphal, C.J., 2001. Dispersal potential and early growth in 14 tropical mangroves: do early life history traits correlate with patterns of adult distribution?: *early life history of tropical mangroves*. J. Ecol. 89, 648–659. https://doi.org/10.1046/j.0022-0477.2001.00584.x.

Cleveland, R.B., Cleveland, W.S., Terpenning, I., 1990. STL: a seasonal-trend decomposition procedure based on loess. J. Off. Stat. 6, 3.

Oceans and coastal ecosystems and their services. In: Cooley, S.R., Schoeman, D.S., Bopp, L., Boyd, P., Donner, S., Ito, S.-I., Wolfgang, K., Martinetto, P., Ojea, E., Racault, M.-F., Rost, B., Skern-Mauritzen, M. (Eds.), 2022. Climate Change 2022: Impacts, Adaptation and Vulnerability. Contribution of Working Group II to the Sixth Assessment Report of the Intergovernmental Panel on Climate Change. Cambridge University Press, Cambridge, United Kingdom ; New York, NY, pp. 379–550. https://doi.org/10.1017/9781009325844.005.

Curnick, D.J., Pettorelli, N., Amir, A.A., Balke, T., Barbier, E.B., Crooks, S., Dahdouh-Guebas, F., Duncan, C., Endsor, C., Friess, D.A., Quarto, A., Zimmer, M., Lee, S.Y., 2019. The value of small mangrove patches. Science 363. https://doi.org/10.1126/science.aaw0809, 239–239.

Dahdouh-Guebas, F., Friess, D.A., Lovelock, C.E., Connolly, R.M., Feller, I.C., Rogers, K., Cannicci, S., 2022. Cross-cutting research themes for future mangrove forest research. Nat. Plants 8, 1131–1135. https://doi.org/10.1038/s41477-022-01245-4.

Dahdouh-Guebas, F., Jayatissa, L.P., Di Nitto, D., Bosire, J.O., Lo Seen, D., Koedam, N., 2005. How effective were mangroves as a defence against the recent tsunami? Curr. Biol. 15, R443–R447. https://doi.org/10.1016/j.cub.2005.06.008.

Das, S., Vincent, J.R., 2009. Mangroves protected villages and reduced death toll during Indian super cyclone. Proc. Natl. Acad. Sci. USA 106, 7357–7360. https://doi.org/10.1073/pnas.0810440106.

Deltares, 2021. In: Delft3D Flexible Mesh Suite: D-Flow Flexible Mesh, 0.9.1. Deltares, Delft.

Di Nitto, D., Erftemeijer, P.L.A., van Beek, J.K.L., Dahdouh-Guebas, F., Higazi, L., Quisthoudt, K., Jayatissa, L.P., Koedam, N., 2013. Modelling drivers of mangrove propagule dispersal and restoration of abandoned shrimp farms. Biogeosciences 10, 5095–5113. https://doi.org/10.5194/bg-10-5095-2013.

Doyle, T.W., Smith III, T.J., Robblee, M.B., 1995. Wind damage effects of Hurricane Andrew on mangrove communities along the southwest coast of Florida, USA. J. Coast Res. 159–168.

Drexler, J.Z., 2001. Maximum longevities of Rhizophora apiculata and R. mucronata propagules. Pac. Sci. 55, 17–22. https://doi.org/10.1353/psc.2001.0004.

Du, Q., Qin, Z., Ming, S., Zhang, C., 2021. Differences in the vertical accretion of sediment among mangrove species with different aerial root types. Estuar. Coast Shelf Sci. 256, 107375 https://doi.org/10.1016/j.ecss.2021.107375.

Duarte, C.M., Losada, I.J., Hendriks, I.E., Mazarrasa, I., Marbà, N., 2013. The role of coastal plant communities for climate change mitigation and adaptation. Nat. Clim. Change 3, 961–968. https://doi.org/10.1038/nclimate1970.

Duke, N., Bunt, J., Williams, W., 1984. Observations on the floral and vegetative phenologies of north-eastern Australian mangroves. Aust. J. Bot. 32, 87–99.

Duke, N.C., 1990. Phenological trends with latitude in the mangrove tree Avicennia marina. J. Ecol. 78, 113–133. https://doi.org/10.2307/2261040.

Duke, N.C., Ball, M.C., Ellison, J.C., 1998. Factors influencing biodiversity and distributional gradients in mangroves. Global Ecol. Biogeogr. Lett. 7, 27–47.

Ellison, A.M., Felson, A.J., Friess, D.A., 2020. Mangrove rehabilitation and restoration as experimental adaptive management. Front. Mar. Sci. 7, 327. https://doi.org/10.3389/fmars.2020.00327.

Ellison, J.C., Buffington, K.J., Thorne, K.M., Gesch, D., Irwin, J., Danielson, J., 2022. Elevations of mangrove forests of Pohnpei, Micronesia. Estuar. Coast Shelf Sci. 268, 107780 https://doi.org/10.1016/j.ecss.2022.107780.

Fairchild, T.P., Bennett, W.G., Smith, G., Day, B., Skov, M.W., Möller, I., Beaumont, N., Karunarathna, H., Griffin, J.N., 2021. Coastal wetlands mitigate storm flooding and associated costs in estuaries. Environ. Res. Lett. 16, 074034 https://doi.org/10.1088/1748-9326/ac0c45.

Fanous, M., Daneshkhah, A., Eden, J.M., Remesan, R., Palade, V., 2023. Hydro-morphodynamic modelling of mangroves imposed by tidal waves using finite element discontinuous Galerkin method. Coast. Eng. 182, 104303 https://doi.org/10.1016/j.coastaleng.2023.104303.

Furukawa, K., Wolanski, E., 1996. Sedimentation in mangrove forests. Mangroves Salt Marshes 1, 3–10. https://doi.org/10.1023/A:1025973426404.

Furusawa, T., Fuchigami, Y., Kobayashi, S., Yokota, M., 2013. Evaluation of mangrove biomass changes due to different human activities in batam island, Indonesia, determined using MODIS EVI and ASTER data. People Cult. Ocean. 29, 35–50.

Gardiner, B., Byrne, K., Hale, S., Kamimura, K., Mitchell, S.J., Peltola, H., Ruel, J.-C., 2008. A review of mechanistic modelling of wind damage risk to forests. Forestry 81, 447–463. https://doi.org/10.1093/forestry/cpn022.

Grueters, U., Ibrahim, M.R., Satyanarayana, B., Dahdouh-Guebas, F., 2019. Individual-based modeling of mangrove forest growth: MesoFON – recent calibration and future direction. Estuar. Coast Shelf Sci., 106302 https://doi.org/10.1016/j.ecss.2019.106302.

Grueters, U., Seltmann, T., Schmidt, H., Horn, H., Pranchai, A., Vovides, A.G., Peters, R., Vogt, J., Dahdouh-Guebas, F., Berger, U., 2014. The mangrove forest dynamics model mesoFON. Ecol. Model. 291, 28–41. https://doi.org/10.1016/j.ecolmodel.2014.07.014.

Hijuelos, A.C., Dijkstra, J.T., Carruthers, T.J.B., Heynert, K., Reed, D.J., van Wesenbeeck, B.K., 2019. Linking management planning for coastal wetlands to potential future wave attenuation under a range of relative sea-level rise scenarios. PLoS One 14, e0216695. https://doi.org/10.1371/journal.pone.0216695.

Horstman, E.M., Dohmen-Janssen, C.M., Bouma, T.J., Hulscher, S.J.M.H., 2015. Tidal-scale flow routing and sedimentation in mangrove forests: combining field data and numerical modelling. Geomorphology 228, 244–262. https://doi.org/10.1016/j.geomorph.2014.08.011.

Hutton, E., Piper, M., Tucker, G., 2020. The Basic Model Interface 2.0: a standard interface for coupling numerical models in the geosciences. J. Open Source Softw. 5, 2317. https://doi.org/10.21105/joss.02317.

Jayanthi, M., Samynathan, M., Thirumurthy, S., Duraismay, M., Kabiraj, S., Vijayakumar, S., Panigrahi, A., Kumaran, M., Muralidhar, M., 2022. Is aquaculture development responsible for mangrove conversion in India? - a geospatial study to assess the influence of natural and anthropogenic factors on mangroves in the last three decades. Aquaculture 561, 738696. https://doi.org/10.1016/j.aquaculture.2022.738696.

Jayatissa, L.P., Wickramasinghe, W.A.A.D.L., Dahdouh-Guebas, F., Huxham, M., 2008. Interspecific variations in responses of mangrove seedlings to two contrasting salinities. Int. Rev. Hydrobiol. 93, 700–710. https://doi.org/10.1002/iroh.200711017.

Jennerjahn, T.C., Jänen, I., Propp, C., Adi, S., Nugroho, S.P., 2013. Environmental impact of mud volcano inputs on the anthropogenically altered Porong River and Madura Strait coastal waters, Java, Indonesia. Estuar. Coast Shelf Sci. 130, 152–160. https://doi.org/10.1016/j.ecss.2013.04.007.

Jiménez, J.A., 1992. 16 - mangrove forests of the pacific coast of Central America. In: Seeliger, U. (Ed.), Coastal Plant Communities of Latin America. Academic Press, San Diego, pp. 259–267. https://doi.org/10.1016/B978-0-08-092567-7.50022-2.

Kamruzzaman, Md, Sharma, S., Hagihara, A., 2013. Vegetative and reproductive phenology of the mangrove *Kandelia obovata*: phenology of *KANDELIA obovata*. Plant Species Biol. 28, 118–129. https://doi.org/10.1111/j.1442-1984.2012.00367.x.

Kathiresan, K., Rajendran, N., 2005. Coastal mangrove forests mitigated tsunami. Estuar. Coast Shelf Sci. 65, 601–606. https://doi.org/10.1016/j.ecss.2005.06.022.

Kirezci, E., Young, I.R., Ranasinghe, R., Muis, S., Nicholls, R.J., Lincke, D., Hinkel, J., 2020. Projections of global-scale extreme sea levels and resulting episodic coastal flooding over the 21st Century. Sci. Rep. 10, 11629 https://doi.org/10.1038/s41598-020-67736-6.

Krauss, K.W., Lovelock, C.E., McKee, K.L., López-Hoffman, L., Ewe, S.M.L., Sousa, W.P., 2008. Environmental drivers in mangrove establishment and early development: a review. Aquat. Bot. 89, 105–127. https://doi.org/10.1016/j.aquabot.2007.12.014.

Krauss, K.W., McKee, K.L., Lovelock, C.E., Cahoon, D.R., Saintilan, N., Reef, R., Chen, L., 2014. How mangrove forests adjust to rising sea level. New Phytol. 202, 19–34. https://doi.org/10.1111/nph.12605.

Krauss, K.W., Osland, M.J., 2019. Tropical cyclones and the organization of mangrove forests: a review. Ann. Bot. mcz161 https://doi.org/10.1093/aob/mcz161.

Lagomasino, D., Price, R.M., Whitman, D., Campbell, P.K.E., Melesse, A., 2014. Estimating major ion and nutrient concentrations in mangrove estuaries in Everglades National Park using leaf and satellite reflectance. Remote Sens. Environ. 154, 202–218. https://doi.org/10.1016/j.rse.2014.08.022.

Lovelock, C.E., Ball, M.C., Feller, I.C., Engelbrecht, B.M.J., Ling Ewe, M., 2006. Variation in hydraulic conductivity of mangroves: influence of species, salinity, and nitrogen and phosphorus availability. Physiol. Plantarum 127, 457–464. https://doi.org/10.1111/j.1399-3054.2006.00723.x.

Lovelock, C.E., Cahoon, D.R., Friess, D.A., Guntenspergen, G.R., Krauss, K.W., Reef, R., Rogers, K., Saunders, M.L., Sidik, F., Swales, A., Saintilan, N., Thuyen, L.X., Triet, T., 2015. The vulnerability of Indo-Pacific mangrove forests to sea-level rise. Nature 526, 559–563. https://doi.org/10.1038/nature15538.

Lovelock, C.E., Feller, I.C., Reef, R., Hickey, S., Ball, M.C., 2017. Mangrove dieback during fluctuating sea levels. Sci. Rep. 7, 1680. https://doi.org/10.1038/s41598-017-01927-6.

Lugo, A.E., Snedaker, S.C., 1974. The ecology of mangroves. Annu. Rev. Ecol. Systemat. 5, 39–64. https://doi.org/10.1146/annurev.es.05.110174.000351.

Magnan, A.K., Oppenheimer, M., Garschagen, M., Buchanan, M.K., Duvat, V.K.E., Forbes, D.L., Ford, J.D., Lambert, E., Petzold, J., Renaud, F.G., Sebesvari, Z., van de Wal, R.S.W., Hinkel, J., Pörtner, H.-O., 2022. Sea level rise risks and societal adaptation benefits in low-lying coastal areas. Sci. Rep. 12, 10677 https://doi.org/10.1038/s41598-022-14303-w.

Maza, M., Lara, J.L., Losada, I.J., 2021. Predicting the evolution of coastal protection service with mangrove forest age. Coast. Eng. 168, 103922 https://doi.org/10.1016/j.coastaleng.2021.103922.

Mazda, Y., Magi, M., Ikeda, Y., Kurokawa, T., Asano, T., 2006. Wave reduction in a mangrove forest dominated by Sonneratia sp. Wetl. Ecol. Manag. 14, 365–378. https://doi.org/10.1007/s11273-005-5388-0.

Mazda, Y., Wolanski, E., King, B., Sase, A., Ohtsuka, D., Magi, M., 1997. Drag force due to vegetation in mangrove swamps. Mangroves Salt Marshes 1, 193–199.

McKee, K.L., 2011. Biophysical controls on accretion and elevation change in Caribbean mangrove ecosystems. Estuar. Coast Shelf Sci. 91, 475–483. https://doi.org/10.1016/j.ecss.2010.05.001.

Merkens, J.-L., Reimann, L., Hinkel, J., Vafeidis, A.T., 2016. Gridded population projections for the coastal zone under the Shared Socioeconomic Pathways. Global Planet. Change 145, 57–66. https://doi.org/10.1016/j.gloplacha.2016.08.009.

Morris, RebeccaL., Strain, E.M.A., Konlechner, T.M., Fest, B.J., Kennedy, D.M., Arndt, S. K., Swearer, S.E., 2019. Developing a nature-based coastal defence strategy for Australia. Aust. J. Civ. Eng. 17, 167–176. https://doi.org/10.1080/14488353.2019.1661062.

Mullarney, J.C., Henderson, S.M., Reyns, J.A.H., Norris, B.K., Bryan, K.R., 2017. Spatially varying drag within a wave-exposed mangrove forest and on the adjacent tidal flat. Continent. Shelf Res. 147, 102–113. https://doi.org/10.1016/j.csr.2017.06.019.

Murray, N.J., Phinn, S.R., DeWitt, M., Ferrari, R., Johnston, R., Lyons, M.B., Clinton, N., Thau, D., Fuller, R.A., 2019. The global distribution and trajectory of tidal flats. Nature 565, 222–225. https://doi.org/10.1038/s41586-018-0805-8.

Narayan, S., Beck, M.W., Reguero, B.G., Losada, I.J., van Wesenbeeck, B., Pontee, N., Sanchirico, J.N., Ingram, J.C., Lange, G.-M., Burks-Copes, K.A., 2016. The effectiveness, costs and coastal protection benefits of natural and nature-based defences. PLoS One 11, e0154735. https://doi.org/10.1371/journal.pone.0154735.

Norris, B.K., Mullarney, J.C., Bryan, K.R., Henderson, S.M., 2021. Relating millimeter-scale turbulence to meter-scale subtidal erosion and accretion across the fringe of a coastal mangrove forest. Earth Surf. Process. Landf. esp. 5047 https://doi.org/10.1002/esp.5047.

Norris, B.K., Mullarney, J.C., Bryan, K.R., Henderson, S.M., 2017. The effect of pneumatophore density on turbulence: a field study in a Sonneratia -dominated mangrove forest. Vietnam. Cont. Shelf Res. 147, 114–127. https://doi.org/10.1016/j.csr.2017.06.002.

Osland, M.J., Feher, L.C., Griffith, K.T., Cavanaugh, K.C., Enwright, N.M., Day, R.H., Stagg, C.L., Krauss, K.W., Howard, R.J., Grace, J.B., Rogers, K., 2017. Climatic controls on the global distribution, abundance, and species richness of mangrove forests. Ecol. Monogr. 87, 341–359. https://doi.org/10.1002/ecm.1248.

Pennings, Steven C., Glazner, Rachael M., Hughes, Zoe J., Kominoski, John S., Armitage, Anna R., April 2021. Effects of Mangrove Cover on Coastal Erosion during a Hurricane in Texas, USA. Ecology 102. https://doi.org/10.1002/ecy.3309.

Peters, R., Vovides, A.G., Luna, S., Grüters, U., Berger, U., 2014. Changes in allometric relations of mangrove trees due to resource availability – a new mechanistic modelling approach. Ecol. Model. 283, 53–61. https://doi.org/10.1016/j.ecolmodel.2014.04.001.

Piou, C., Feller, I.C., Berger, U., Chi, F., 2006. Zonation patterns of Belizean offshore mangrove forests 41 Years after a catastrophic Hurricane1. Biotropica 38, 365–374. https://doi.org/10.1111/j.1744-7429.2006.00156.x.

Pretzsch, H., 2009. Forest Dynamics, Growth and Yield: from Measurement to Model. Springer Berlin Heidelberg, Berlin, Heidelberg. https://doi.org/10.1007/978-3-540-88307-4.

Rabinowitz, D., 1978. Dispersal properties of mangrove propagules. Biotropica 10, 47. https://doi.org/10.2307/2388105.

Richards, D.R., Friess, D.A., 2016. Rates and drivers of mangrove deforestation in Southeast Asia, 2000–2012. Proc. Natl. Acad. Sci. USA 113, 344–349. https://doi.org/10.1073/pnas.1510272113.

Rivera-Monroy, V.H., Zhao, X., Wang, H., Xue, Z.G., 2022. Are existing modeling tools useful to evaluate outcomes in mangrove restoration and rehabilitation projects? A Minireview. Forests 13, 1638. https://doi.org/10.3390/f13101638.

Rodríguez, J.F., Saco, P.M., Sandi, S., Saintilan, N., Riccardi, G., 2017. Potential increase in coastal wetland vulnerability to sea-level rise suggested by considering hydrodynamic attenuation effects. Nat. Commun. 8, 16094 https://doi.org/10.1038/ncomms16094.

Rogers, K., 2021. Accommodation space as a framework for assessing the response of mangroves to relative sea-level rise. Singapore J. Trop. Geogr. 42, 163–183. https://doi.org/10.1111/sjtg.12357.

Schoonees, T., Gijón Mancheño, A., Scheres, B., Bouma, T.J., Silva, R., Schlurmann, T., Schüttrumpf, H., 2019. Hard structures for coastal protection, towards greener designs. Estuar. Coast 42, 1709–1729. https://doi.org/10.1007/s12237-019-00551-z.

Seabold, S., Perktold, J., 2010. Statsmodels: econometric and statistical modeling with Python. Presented at the. In: Python in Science Conference, pp. 92–96. https://doi.org/10.25080/Majora-92bf1922-011. Austin, Texas.

Setiawan, A., Realino, B., Triyulianti, I., Hamzah, F., Murdimanto, A., Putri, M.R., Nugroho, D., 2019. Using WorldView-2 imagery to estimate mangroves density in the Porong estuary. In: Barale, V., Gade, M. (Eds.), Remote Sensing of the Asian Seas. Springer International Publishing, Cham, pp. 377–393. https://doi.org/10.1007/978-3-319-94067-0_21.

Sharma, S., Hoque, A.T.M.R., Analuddin, K., Hagihara, A., 2014. A model of seasonal foliage dynamics of the subtropical mangrove species Rhizophora stylosa Griff. growing at the northern limit of its distribution. For. Ecosyst. 1, 15. https://doi.org/10.1186/s40663-014-0015-2.

Shih, S.-S., Huang, Z.-Z., Hsu, Y.-W., 2022. Nature-based solutions on floodplain restoration with coupled propagule dispersal simulation and stepping-stone approach to predict mangrove encroachment in an estuary. Sci. Total Environ. 851, 158097 https://doi.org/10.1016/j.scitotenv.2022.158097.

Sidik, F., Hidayatullah, T., Kadarisman, H.P., Lovelock, C.E., 2013. Evaluation of mangrove development in a created mangrove wetland in Porong, East Java. In: Regional Symposium on Mangrove Ecosystem Management in Southeast Asia. Presented at the Mainstreaming Mangroves. Ministry of Forestry Indonesia, Surabaya, Indonesia.

Sidik, F., Neil, D., Lovelock, C.E., 2016. Effect of high sedimentation rates on surface sediment dynamics and mangrove growth in the Porong River, Indonesia. Mar. Pollut. Bull. 107, 355–363. https://doi.org/10.1016/j.marpolbul.2016.02.048.

Slim, F., Gwada, P., Kodjo, M., Hemminga, M., 1996. Biomass and litterfall of Ceriops tagal and Rhizophora mucronata in the mangrove forest of Gazi Bay, Kenya. Mar. Freshw. Res. 47, 999–1007.

Spalding, M.D., McIvor, A.L., Beck, M.W., Koch, E.W., Möller, I., Reed, D.J., Rubinoff, P., Spencer, T., Tolhurst, T.J., Wamsley, T.V., Wesenbeeck, B.K., Wolanski, E., Woodroffe, C.D., 2014. Coastal ecosystems: a critical element of risk reduction. Conserv. Lett. 7, 293–301. https://doi.org/10.1111/conl.12074.

Srivastava, P.B.L., Khamis, D., 1978. Progress of natural regeneration after final felling under the current silvicultural practices in matang mangrove reserve. Pertanika 2, 126–135.

Sudhir, S., Arunprasath, A., Sankara Vel, V., 2022. A critical review on adaptations, and biological activities of the mangroves. J. Nat. Pestic. Res. 1, 100006 https://doi.org/10.1016/j.napere.2022.100006.

Suwa, R., Hagihara, A., 2008. Seasonal changes in canopy photosynthesis and foliage respiration in a Rhizophora stylosa stand at the northern limit of its natural distribution. Wetl. Ecol. Manag. 16, 313–321. https://doi.org/10.1007/s11273-007-9066-2.

Tala, W.D.S., 2020. The study of mangrove reproductive phenology in the Rhizophoraceae family (Bruguiera gymnorrhiza (L.) lamk., ceriops tagal (perr.) C.B. Rob., Rhizophora apiculata blume. And Rhizophora mucronata lamk.). J. Biol. Trop. 20, 406–415. https://doi.org/10.29303/jbt.v20i3.2091.

Temmerman, S., Horstman, E.M., Krauss, K.W., Mullarney, J.C., Pelckmans, I., Schoutens, K., 2023. Marshes and mangroves as nature-based coastal storm buffers. Ann. Rev. Mar. Sci 15. https://doi.org/10.1146/annurev-marine-040422-092951 annurev-marine-040422-092951.

Temmerman, S., Meire, P., Bouma, T.J., Herman, P.M.J., Ysebaert, T., De Vriend, H.J., 2013. Ecosystem-based coastal defence in the face of global change. Nature 504, 79–83. https://doi.org/10.1038/nature12859.

Twilley, R.R., Rivera-Monroy, V.H., 2005. Developing performance measures of mangrove wetlands using simulation models of hydrology, nutrient biogeochemistry, and community dynamics. J. Coast Res. 79–93.

Van der Stocken, T., Wee, A.K.S., De Ryck, D.J.R., Vanschoenwinkel, B., Friess, D.A., Dahdouh-Guebas, F., Simard, M., Koedam, N., Webb, E.L., 2019. A general framework for propagule dispersal in mangroves: a general framework for propagule dispersal in mangroves. Biol. Rev. 94, 1547–1575. https://doi.org/10.1111/brv.12514.

van der Wegen, M., Roelvink, J.A., 2008. Long-term morphodynamic evolution of a tidal embayment using a two-dimensional, process-based model. J. Geophys. Res. 113 https://doi.org/10.1029/2006JC003983.

van Hespen, R., Hu, Z., Borsje, B., De Dominicis, M., Friess, D.A., Jevrejeva, S., Kleinhans, M., Maza, M., van Bijsterveldt, C.E.J., Van der Stocken, T., van Wesenbeeck, B., Xie, D., Bouma, T.J., 2022a. Mangrove forests as a nature-based solution for coastal flood protection: biophysical and ecological considerations. Water Sci. Eng. https://doi.org/10.1016/j.wse.2022.10.004.

van Hespen, R., Hu, Z., Peng, Y., Borsje, B.W., Kleinhans, M., Ysebaert, T., Bouma, T.J., 2021. Analysis of coastal storm damage resistance in successional mangrove species. Limnol. Oceanogr. 66, 3221–3236. https://doi.org/10.1002/lno.11875.

van Hespen, R., Hu, Z., Peng, Y., Zhu, Z., Ysebaert, T., Bouma, T.J., 2022b. Identifying trait-based tolerance to sediment dynamics during seedling establishment across eight mangrove species. Limnol. Oceanogr. lno. 12202 https://doi.org/10.1002/lno.12202.

van Maanen, B., Coco, G., Bryan, K.R., 2015. On the ecogeomorphological feedbacks that control tidal channel network evolution in a sandy mangrove setting. Proc. R. Soc. Math. Phys. Eng. Sci. 471, 20150115 https://doi.org/10.1098/rspa.2015.0115.

van Wesenbeeck, B.K., de Boer, W., Narayan, S., van der Star, W.R.L., de Vries, M.B., 2017. Coastal and riverine ecosystems as adaptive flood defenses under a changing climate. Mitig. Adapt. Strategies Glob. Change 22, 1087–1094. https://doi.org/10.1007/s11027-016-9714-z.

Vincenot, C.E., Mazzoleni, S., Parrott, L., 2016. Editorial: hybrid solutions for the modeling of complex environmental systems. Front. Environ. Sci. 4 https://doi.org/10.3389/fenvs.2016.00053.

Vizcaya-Martínez, D.A., Flores-de-Santiago, F., Valderrama-Landeros, L., Serrano, D., Rodríguez-Sobreyra, R., Álvarez-Sánchez, L.F., Flores-Verdugo, F., 2022. Monitoring detailed mangrove hurricane damage and early recovery using multisource remote

sensing data. J. Environ. Manag. 320, 115830 https://doi.org/10.1016/j.jenvman.2022.115830.
Wafar, S., Untawale, A.G., Wafar, M., 1997. Litter fall and energy flux in a mangrove ecosystem. Estuar. Coast Shelf Sci. 44, 111–124. https://doi.org/10.1006/ecss.1996.0152.
Wan, Y., Wan, L., Li, Y., Doering, P., 2017. Decadal and seasonal trends of nutrient concentration and export from highly managed coastal catchments. Water Res. 115, 180–194. https://doi.org/10.1016/j.watres.2017.02.068.
Wang, W.J., He, H.S., Fraser, J.S., Thompson, F.R., Shifley, S.R., Spetich, M.A., 2014. Landis pro: a landscape model that predicts forest composition and structure changes at regional scales. Ecography 37, 225–229. https://doi.org/10.1111/j.1600-0587.2013.00495.x.
Willemsen, P.W.J.M., Horstman, E.M., Borsje, B.W., Friess, D.A., Dohmen-Janssen, C.M., 2016. Sensitivity of the sediment trapping capacity of an estuarine mangrove forest. Geomorphology 273, 189–201. https://doi.org/10.1016/j.geomorph.2016.07.038.
Wilson, P., 2020. A-Z of Tree Terms: A Companion to British Arboriculture, third ed.), Third. ed. Ethelburga House.
Wimmler, M.-C., Bathmann, J., Peters, R., Jiang, J., Walther, M., Lovelock, C.E., Berger, U., 2021. Plant–soil feedbacks in mangrove ecosystems: establishing links between empirical and modelling studies. Trees (Berl.) 35, 1423–1438. https://doi.org/10.1007/s00468-021-02182-z.
Wirjoadmodjo, H., Hamzah, Z., 1982. Beberapa pengalaman perum perhutani dalam pengelolaan hutan mangrove. In: Prosiding Seminar Ekosistem Mangrove. Presented at the Ekosistem Mangrove, Balai Penelitian Hutan, Perum Perhutani, Biotrop, Dit. Bina Program Kehutanan, Jakarta.
Coastal systems and low-lying areas. In: Wong, P.P., Losada, I.J., Gattuso, J.-P., Hinkel, J., Khattabi, A., McInnes, K.L., Saito, Y., Sallenger, A. (Eds.), 2014. Climate Change 2014: Impacts, Adaptation, and Vulnerability. Part A: Global and Sectoral Aspects. Contribution of Working Group II to the Fifth Assessment Report of the Intergovernmental Panle on Climate Change. Cambridge University Press, Cambridge, United Kingdom ; New York, NY, pp. 361–409.
Woodroffe, C., 1992. Mangrove sediments and geomorphology. In: Robertson, A.I., Alongi, D.M. (Eds.), Tropical Mangrove Ecosystems, Coastal and Estuarine Studies. American Geophysical Union, Washington, D. C., pp. 7–41. https://doi.org/10.1029/CE041p0007
Woodroffe, C.D., Rogers, K., McKee, K.L., Lovelock, C.E., Mendelssohn, I.A., Saintilan, N., 2016. Mangrove sedimentation and response to relative sea-level rise. Ann. Rev. Mar. Sci 8, 243–266. https://doi.org/10.1146/annurev-marine-122414-034025.
World Bank, 2017. Implementing Nature Based Flood Protection : Principles and Implementation Guidance (Working Paper). World Bank, Washington DC, USA.
Xie, D., Schwarz, C., Brückner, M.Z.M., Kleinhans, M.G., Urrego, D.H., Zhou, Z., van Maanen, B., 2020. Mangrove diversity loss under sea-level rise triggered by bio-morphodynamic feedbacks and anthropogenic pressures. Environ. Res. Lett. 15, 114033 https://doi.org/10.1088/1748-9326/abc122.
Xie, D., Schwarz, C., Kleinhans, M.G., Zhou, Z., van Maanen, B., 2022. Implications of coastal conditions and sea-level rise on mangrove vulnerability: a bio-morphodynamic modelling study. J. Geophys. Res. Earth Surf. 127, e2021JF006301 https://doi.org/10.1029/2021JF006301.
Zainol, Z., Peris, A.D., Akhir, M.F., Rahim, N.H.A., Satyanarayana, B., Dahdouh-Guebas, F., 2022. Mangrove propagule dispersal in a shallow and narrow coastal lagoon: a simulation-based assessment of the setiu wetlands, Malaysia. Forests 13, 1525. https://doi.org/10.3390/f13091525.
Zhang, K., Thapa, B., Ross, M., Gann, D., 2016. Remote sensing of seasonal changes and disturbances in mangrove forest: a case study from South Florida. Ecosphere 7. https://doi.org/10.1002/ecs2.1366.